Water Level Modulation of Wave Transformation, Setup and Runup Over La Saline Fringing Reef

Bruch, William ; Cordier, Emmanuel ; Floc'h, France ; Pearson, Stuart

DOI
10.1029/2022JC018570

Publication date
2022

Document Version
Final published version

Published in
Journal of Geophysical Research: Oceans

Citation (APA)
Bruch, W., Cordier, E., Floc'h, F., & Pearson, S. (2022). Water Level Modulation of Wave Transformation, Setup and Runup Over La Saline Fringing Reef. *Journal of Geophysical Research: Oceans*, *127*(7), 1-23. Article e2022JC018570. https://doi.org/10.1029/2022JC018570

JGR Oceans

RESEARCH ARTICLE
10.1029/2022JC018570

Water Level Modulation of Wave Transformation, Setup and Runup Over La Saline Fringing Reef

William Bruch[1,2], Emmanuel Cordier[3], France Floc'h[1], and Stuart G. Pearson[4,5]

[1]Univ Brest, CNRS, Géo-Océan, UMR6538, Plouzané, France, [2]Ecole Centrale de Nantes, CNRS, LHEEA, UMR6598, Nantes, France, [3]Observatoire des Sciences de l'Univers de La Réunion (OSU-R), UAR3365, Saint Denis, France, [4]Faculty of Civil Engineering and Geosciences, Delft University of Technology, Delft, The Netherlands, [5]Department of Applied Morphodynamics, Deltares, Delft, The Netherlands

Key Points:

- Study of wave transformation over La Saline fringing reef, a natural coastal defense against Southern Ocean swell and cyclonic events
- As gravity waves dissipate over the fringing reef, significant energy transfer to infragravity and very low frequency bands occurs
- Wave setup and runup are greater for higher offshore wave height (H_{s0}) and lower water level. Modeled runup scales as ≈20% of H_{s0}

Correspondence to:

F. Floc'h,
france.floch@univ-brest.fr

Citation:

Bruch, W., Cordier, E., Floc'h, F., & Pearson, S. G. (2022). Water level modulation of wave transformation, setup and runup over La Saline fringing reef. *Journal of Geophysical Research: Oceans*, *127*, e2022JC018570. https://doi.org/10.1029/2022JC018570

Received 19 FEB 2022
Accepted 19 JUN 2022

Author Contributions:

Conceptualization: Emmanuel Cordier, France Floc'h
Data curation: Emmanuel Cordier
Formal analysis: William Bruch, Emmanuel Cordier, France Floc'h
Funding acquisition: Emmanuel Cordier, France Floc'h
Investigation: William Bruch, Emmanuel Cordier, France Floc'h
Methodology: William Bruch, Emmanuel Cordier, France Floc'h
Project Administration: William Bruch, Emmanuel Cordier, France Floc'h
Resources: Emmanuel Cordier, France Floc'h
Software: William Bruch, Emmanuel Cordier, France Floc'h

Abstract Coral reefs represent an efficient natural mechanical coastal defense against ocean waves. The focus of this study is La Saline fringing coral reef, located in the microtidal West of La Réunion Island in the Indian Ocean, frequently exposed to Southern Ocean swell and cyclonic events. The aim is to provide a better understanding of the reef's coastal defense characteristics for several Southern Ocean swell events. Pressure sensors were placed across the reef to measure water level fluctuations and to study wave transformation. A numerical model (XBeach surfbeat), validated using field observations, was used to deepen understanding of wave transformation, wave setup and runup. Field measurements and model outputs show that as gravity waves dissipate over the reef, and frequency-dependent dissipation of infragravity waves by bottom-friction occurs, the reef acts as a low-pass filter. Wave-induced setup is found to be the dominant hydrodynamic component. Setup and runup are each 98% and 79% driven by the offshore significant wave height, and 2% and 21% driven by the tide. The modulation of the water level by setup is the main contributor to runup in the fringing reef. At semidiurnal timescales, setup and runup are in antiphase with tidal variations as lower water levels result in higher gravity wave energy dissipation, setup and runup. Simple-to-use transfer functions relating incident wave characteristics to these hydrodynamic components are proposed. The effects of bottom friction and water level on the defensive capacity of the coral reef highlight future implications of structural damage and sea level rise.

Plain Language Summary Coral reefs protect the coastline from ocean waves. The protective characteristics of reefs are site-dependent as they vary according to a number of parameters such as coral health, water depth, oceanic and meteorological conditions. La Saline fringing reef on La Reunion Island is frequently exposed to Southern Ocean swell and cyclonic events. Accompanied by numerical modeling efforts, pressure sensors placed across the reef allow to study water level fluctuations for a range of swell events and tides. Results show that waves transform as they break and dissipate over the reef, as the energy of higher-frequency waves is transferred toward lower frequencies. At the study site, offshore significant wave height is the main driver of the reef hydrodynamics. The tide also contributes by modulating the water level over the reef flat. In the context of predicted sea level rise in recent climate change scenarios, as well as possible reef health decline, present study results suggest that the protective capacity of the La Saline fringing reef could decline, thus altering future reef hydrodynamics and associated sediment transport.

1. Introduction

Low-latitude and often low-lying islands are frequently located in oceanic regions prone to extreme natural events and disasters of hydro-meteorological origin, such as tropical cyclones, storms, flooding, and drought. In the context of global climate change, growing concern for the future of these environments has resulted in recent initiatives (e.g., UNESCO, 2014) for the building of small island resilience. Many of these tropical environments are bordered by coral reefs that are home to some of the most biodiverse and productive ecosystems on the planet (Pascal et al., 2016; Woodhead et al., 2019) and provide extremely valuable ecosystem services as a coastal defense against these events. An increasing number of studies indicate that up to 98% of incident wave energy is dissipated by coral reef systems (Beetham et al., 2016; Brander et al., 2004; Ferrario et al., 2014; A.-C. Péquignet et al., 2011).

Reef systems protect the coastline by inducing wave transformation in incident wave fields through wave-bottom interactions. Reef systems act as a low-pass filter, as wave energy dissipation mainly occurs in the gravity part

Supervision: Emmanuel Cordier, France Floc'h
Validation: William Bruch, Emmanuel Cordier, France Floc'h, Stuart G. Pearson
Visualization: William Bruch, Emmanuel Cordier, France Floc'h, Stuart G. Pearson
Writing – review & editing: William Bruch, Emmanuel Cordier, France Floc'h, Stuart G. Pearson

of the wave spectrum (typically above frequency of 0.04 Hz) through mechanisms such as wave breaking in the surf zone and bottom friction, especially important over rough and shallow reef flats (Ferrario et al., 2014; Lowe et al., 2005; Monismith et al., 2015). These physical processes are strongly related to the water level above the reef crest and to the bed friction (Lentz et al., 2016) which is regularly described by two coefficients in reef environments. The short period wave friction coefficient (dimensionless, commonly denoted f_w) describes the rate of gravity wave energy dissipation due to bed friction, and is strongly affected by the reef structural complexity (Harris et al., 2018). f_w is most often found over the 0.1–0.5 range, sometimes reaching significantly higher values, with increasing friction for increasing coral complexity (Lentz et al., 2016). The friction coefficient (commonly denoted c_f) is associated with both the mean currents and the long period waves, and refers to the dissipation of energy in the mean current and wave-induced flow by the reef. c_f is commonly spatially varying, by depending on coral species density (among other properties) and water depth (Pearson et al., 2017; Quataert et al., 2015; van Dongeren et al., 2013). These two coefficients, commonly indirectly calibrated or estimated from cross-reef wave measurements or numerical simulations, strongly depend on the characteristics of each individual study site, thus highlighting the importance of multiplying local in situ studies.

In coastal regions, the dissipation of incident gravity waves (GW) (0.04–0.25 Hz), herein referred to as GW, results in increased water levels over the reef as a result of wave-induced setup (Gerritsen, 1980; Vetter et al., 2010), resulting in the possible flooding of coastal areas. GW dissipation over the reef flat is is often incomplete. Runup, which combines setup and swash to describe the total water level at the shoreline, is commonly related to coastal flooding events and erosion (Butt & Russell, 2000; Pomeroy et al., 2012; Quataert et al., 2015). Runup is related to offshore GW height, period, beach slope (e.g., Ruggiero et al., 2001), setup, and lower frequency wave components (Beetham et al., 2016; Cheriton et al., 2016; Guedes et al., 2013). GW dissipation contributes to the amplification of such longer period wave components (Pomeroy et al., 2012; Sous et al., 2019; Symonds et al., 1982), which include infragravity (IG) (0.004–0.04 Hz) and very low frequency (VLF) (0.001–0.004 Hz) waves, herein referred to as IG and VLF waves, respectively. IG wave generation is associated with the surf-zone-width-dependent breakpoint forcing mechanism, and the gravity wave group mechanism, the latter describing the release of free bound waves from GW envelopes during shoaling and breaking processes. The resulting IG waves have been shown to significantly contribute to bed shear in reef systems as well as overwash, potentially leading to damage to coral reefs (Baumann et al., 2019) as well as shoreline erosion (Bertin et al., 2018). VLF waves are identified as seiche-like and potentially resonating waves formed and amplified by non-linear wave transformation associated with wave-breaking processes (Gawehn et al., 2016; Péquignet et al., 2014; Sous et al., 2019). In strong swell events, GW, IG and VLF combined can strongly contribute to reef hydrodynamics, threatening shoreline and reef structural integrity.

The role of and need for coral reefs as a shield against such hazards is expected to evolve over time. Observations and climate predictions point toward global sea level rise as well as increasingly frequent and intense tropical storms and cyclones (Beetham & Kench, 2018; Cheriton et al., 2016; Grady et al., 2013; McLean & Kench, 2015; Merrifield et al., 2014; Quataert et al., 2015; Storlazzi et al., 2015). Projected increases in carbon dioxide and temperature combined with anthropogenic stresses may lead to the loss of much of the world's coral reefs by the end of the 21st century (Camp et al., 2018; Hoegh-Guldberg et al., 2007; Hughes et al., 2003, 2017, 2018), and with them the natural coastal protection they provide against increasingly severe wave-driven flooding events in tropical islands and atolls (Harris et al., 2018; Principe et al., 2011; Sheppard et al., 2005). If the underlying physical processes of coral reef shore-protection are increasingly understood, their accurate quantification is hindered by the high heterogeneity of reef and shoreline morphologies (e.g., Baldock et al., 2014; van Dongeren et al., 2017) as well as meteorological and oceanic conditions (e.g., Lowe and Falter (2015)). Furthermore, Owen et al. (2016) noted that small variations in island topography and land use also influence wave-driven flooding and associated impacts. Responding to this need for flood predictions over reefs of widely varying shape and size but lacking sufficient field measurements, Pearson et al. (2017) numerically simulated over 174,000 combinations of different reef morphology and physical forcing. They showed that waves, water levels and reef width are the most important parameters to consider when predicting reef wave heights and runup. However, there is still a need for more detailed field observations of such sites (Pearson et al., 2017). Fringing reefs are particularly interesting as their narrow and shallow characteristics can result in the highest setup and runup at the shore front.

In coral reef systems, the wave setup appears to be modulated by the water level (Becker et al., 2014; Bonneton et al., 2007; Sous, Dodet, et al., 2020). Under certain coral reef configurations, water level is either the dominant

influence on lagoon hydrodynamics (Chevalier et al., 2015), or at least modulates dynamics primarily driven by oceanic waves (Becker et al., 2014). Wave runup and the associated swash-zone dynamics and sediment transport are conditioned by the hydrodynamic processes induced by the reef flat, which are projected to change with sea level rise (Shope et al., 2017; Storlazzi et al., 2018). In light of this, this study addresses the question of wave dissipation on La Saline (La Réunion island) fringing reef, and the forcing of local hydrodynamic processes. Since the wave dynamics and tidal fluctuations are shown to be specific to each reef system, this study uses a combined approach between field observations and 1-D numerical modeling (XBeach surfbeat model, Roelvink et al., 2009) in order to investigate the dissipative capacity of this fringing reef. Here, field measurements are made to describe water levels offshore and inside the reef, to estimate the GW dissipation due to bottom friction on the reef, study water level variations, and to validate the numerical model. This model is in turn used to predict runup at the shore. The main objective is to provide transfer functions linking incident waves, tide, setup and runup, which are required by the scientific and engineering community and therefore decision and policy makers for coastal zone management.

2. Field Measurements and Data Analysis

2.1. Study Area and Experiment Design

La Saline fringing reef is located on the western coast of La Réunion Island in the South Western Indian Ocean (SWIO) (Figures 1a and 1b), leeward of the prevailing winds, and is seasonally exposed to winter austral swell events (April to October) and (to a lesser extent) oceanic swell generated by tropical cyclones during the austral summer (November to March) generally impacting the northern shores of the island. The tides around La Réunion are mixed, mainly semi-diurnal with a Mean Tidal Range (MTR) of 0.37 m (Cordier et al., 2013). National Centers for Environmental Prediction (NCEP) 30-year Phase 2 wave hindcasts (NCEP, https://polar.ncep.noaa.gov/waves/) show that the mean peak wave direction is South-Westerly (approximately 225°N), the mean peak period is 13.3 s, and the mean significant wave height is 1.9 m. Maximum values due to extreme swell events can reach 4.2 m and 18.9 s in height and peak period respectively. The winter austral swells are generated by distant storms induced by strong atmospheric depressions that occur in the Southern Ocean at a distance of 3,000–4,000 km from La Réunion (Davy et al., 2016). These swells may produce significant damage to coastal infrastructures such as roads, houses, harbors, but also to the natural coral reef protecting part of the western coast of La Réunion (Cordier et al., 2012). The study site is located in the south part of a 8 km long fringing reef with a convex shape, narrowing in its northern part. The fringing reef is around 500 m wide, backed by a sandy beach of approximately 30 m with a 1:10 slope (Figures 1b and 1c). Our results are specific to this study site by representing the widest part of the whole reef facing to the south-west, whilst other parts of the reef face to the west. From the beach to the reef flat (herein RF), the back reef (approximately 200 m wide, herein BR) has a mean water depth of approximately 1 m and is essentially made up of biodetrital sands occupied by scattered coral colonies. The reef flat has a water depth of about 0.5 m and can sometimes be exposed at low tide. Beyond the RF, the reef-slope (hereafter RS, with a slope nearing 1:15) or fore reef has a rough topography made of individual coral heads, boulders and spurs that reach 20 m depth. The reef crest (0.3 m depth below mean sea level, herein denoted MSL) marks the transition between the RS and the RF, and is where the oceanic incident waves break.

A cross-shore transect of bottom fixed Ocean Sensor System Instrument wave gauges (OSSI) combined with an upward-facing Nortek Aquadopp current profiler (AQP) was deployed for 53 days across La Saline reef from 13-Mar-2017 to 05-May-2017 (Figure 1b). The two OSSI pressure sensors were configured to continuously record the sea states at a sampling frequency of 10 Hz and the AQP was configured in an hourly burst mode, recording 2,048 samples at 2 Hz (≈18 min). The RS station was located on the reef slope at a mean depth of 19.5 m and combined the OSSI with the AQP. The RF station was located in the reef flat at the transition zone with the back-reef, at a mean depth of 0.9 m.

These field data were used to quantify the wave heights in each frequency-band of the wave spectrum, the short-wave dissipation processes due to bottom friction across the reef flat and the induced setup for different conditions of oceanic incident wave heights and tides. The runup, in turn, was extracted from the numerical model (cf. Section 3).

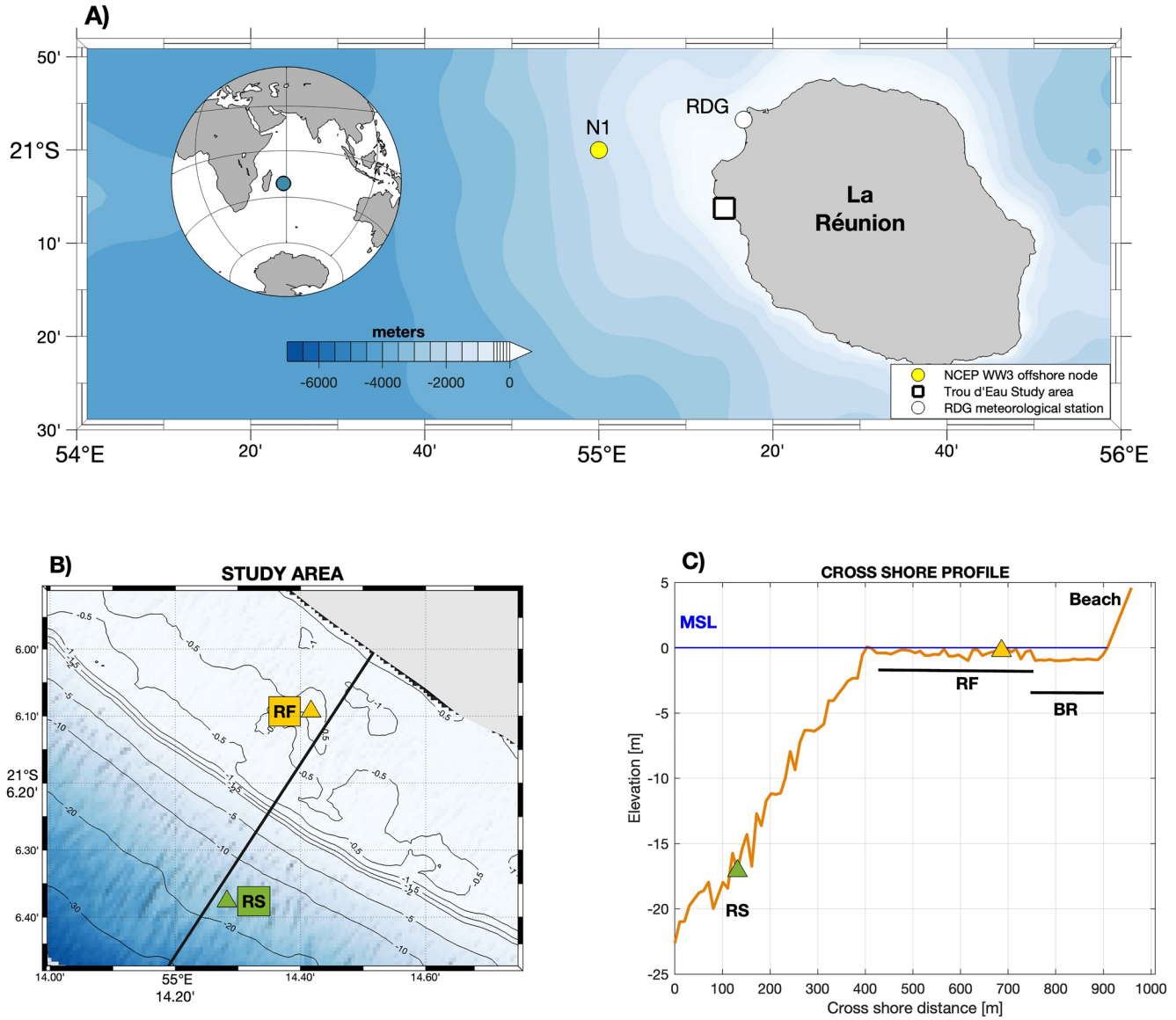

Figure 1. (a) Location of La Reunion island in the South Western Indian Ocean, the studied area is indicated by the white square, the MeteoFrance Rivière des Galets (RDG) meteorological station is indicated by a white dot, (b) zoom on the fringing reef indicating the bathymetry of the fringing reef and the position of the cross-shore transect with the two measurement points on the reef flat (RF) and on the reef slope (RS) separating the open ocean from the back reef (BR), (c) detailed vertical profile of the cross-shore transect used for the 1-D XBeach modeling.

2.2. Data Analysis

The OSSI pressure data were corrected (a) from atmospheric MSL pressure recorded at the MeteoFrance station "La Rivière Des Galets" (≈20 km northward, RDG on Figure 1a) and (b) non-hydrostatic pressure following linear wave theory (Bishop & Donelan, 1987; Hom-ma et al., 1966). The water depths h were extracted from the total signal using a second-order Butterworth low pass filter with a cut-off frequency at 6 hr in order to keep the tidal fluctuations, and averaged over 10 min. The residual high frequency signal was kept for spectral analysis in order to retrieve the energy density spectrum of the sea state $E(f)$ for each of the following 3 frequencies bands: GW (0.04–0.25 Hz), IG waves (0.004–0.04 Hz) and VLF waves (VLF, 0.0006–0.004 Hz). The Fast Fourier Transform method accompanied with Hamming windowing was used and applied over 4,096 continuous data points (nfft) (≈7 min) for GW, and over 32,768 (nfft) (≈55 min) for IG and VLF waves. Finally, to avoid information loss at the edge of each data subsample, a moving average was performed spanning 30 min for GWs and 3 hr

for IG and VLF waves, with 50% overlap (Pierson & Marks, 1952). The AQP data at the RS sample location were finally used to compute incident wave height, peak period and direction using the PUV method (Pedersen, 2002).

The spectral parameters significant wave height H_S, root-mean-square wave height H_{RMS}, and the mean energetic period $T_{m0,-1}$ were calculated in each frequency band according to the equations $H_S = 4\sqrt{m_0}$, $H_{RMS} = \sqrt{8m_0}$ and $T_{m0,-1} = \frac{m_{-1}}{m_0}$ where m_n is the *nth* order moment of the energy density spectrum of the sea state $E(f)$ such that $m_n = \int_0^\infty E(f) f^n df$ (Holthuijsen, 2010). The observed setup (which can be denoted η) in the reef flat η_{RF} was computed from the 10 min averaged water depths h_{RS} and h_{RF} for the RS and RF location respectively, following the Vetter et al. (2010) formula:

$$\eta_{RF} = h_{RF} - h_{RS} - (bt + c) \tag{1}$$

where t is time, b and c are obtained from a regression of the form:

$$h_{RF} - h_{RS} = aH_{RMS}^{RS} + bt + c \tag{2}$$

with H_{RMS}^{RS} the root-mean-square wave height at the reef slope location. This procedure is used to account for relative pressure drift over time between the two sensors, and to select a reference level offset, c, so that the (RF) setup is null $\eta_{RF} = 0$ when the reef slope RMS wave height is null $H_{RMS}^{RS} = 0$. The strength of this relation is quite good with $R^2 = 0.95$, allowing for an accurate estimate of the vertical position of the RS sensor that is $c = 18.7$ m below the RF sensor position.

In order to compute absolute sea level variations according to a referenced datum, an accurate estimate of the vertical position of the pressure sensors is necessary. We used the bathymetric data set illustrated in Figure 1 projected in the WGS84-UTM40S coordinate system and using a local vertical datum reference (IGN89) that corresponds to the MSL. This bathymetric chart is a merged product between a 1 m high resolution topography and bathymetry issued from LIDAR acquisition and a 0.4 m high resolution bathymetry of the shallower parts of the reef issued from hyperspectral images (Mouquet et al., 2016; Ropert Michel et al., 2016). The vertical localization of the reef flat sensor (denoted ZRF) on this gridded data indicates a vertical height of 0.9 m below datum, so that ZRF = −0.9 m. Considering the previously calculated relative position of the RS sensor to RF sensor of 18.7 m, the vertical position of the RS sensor (denoted ZRS) below datum can be deduced, and ZRS = −19.6 m. Finally, the vertical location of the reef crest (denoted ZRC) was also extracted from this bathymetric chart as the highest point between the reef slope and the reef flat, resulting in a reef crest located at a distance $D = 280$ m from the RF sensor and a ZRC = −0.3 m below datum.

2.3. Overview of Oceanic Conditions During Field Observations

In addition to the OSSI field measurements made at the RS station, AQP measurements as well as external global WaveWatch III (WW3) (hereafter WW3) hindcasts (WAVEWATCH III®, Production Hindcast, Multi-grid Data: https://polar.ncep.noaa.gov/waves/hindcasts/prod-multi_1.php) produced by the National Oceanic and Atmospheric Administration (NOAA) and the NCEP are shown in Figure 2, providing an overview of oceanic conditions during the study period. The WW3-modeled significant wave height, peak period and direction were extracted at model node located 25 km west of La Réunion Island, at latitude 21°S and longitude 55°E, illustrated by the node N1 on Figure 1a.

During the 53 days of the experiment, the tide is a typical microtidal regime with a maximum tidal range around 50 cm, a minimum around 4 cm, and a MTR of 27 cm (Figure 2a). The mean tidal level slightly decreased all along the field experiment from +0.1 m to −0.1 m relative to the reference datum. The wave climate captured here is representative of the average wave conditions in the SWIO during the austral winter, and previously described in Section 2.1 (225°N mean wave peak direction, 13.3 s mean peak period, and 1.9 m mean wave height). The linear fit between the modeled and observed data at the reef slope is quite good with $R^2 = 0.87$ and a Root Mean Square Error (RMSE) of 0.19 m when comparing wave heights, and $R^2 = 0.43$ and a RMSE of 1.44 s when comparing peak period. However, the WW3 results slightly overestimate the significant wave heights during most of the weather conditions, and underestimate the wave heights during the double-peaked strong swell event at the end of April. These differences are likely due to the fact that the model is configured for the offshore

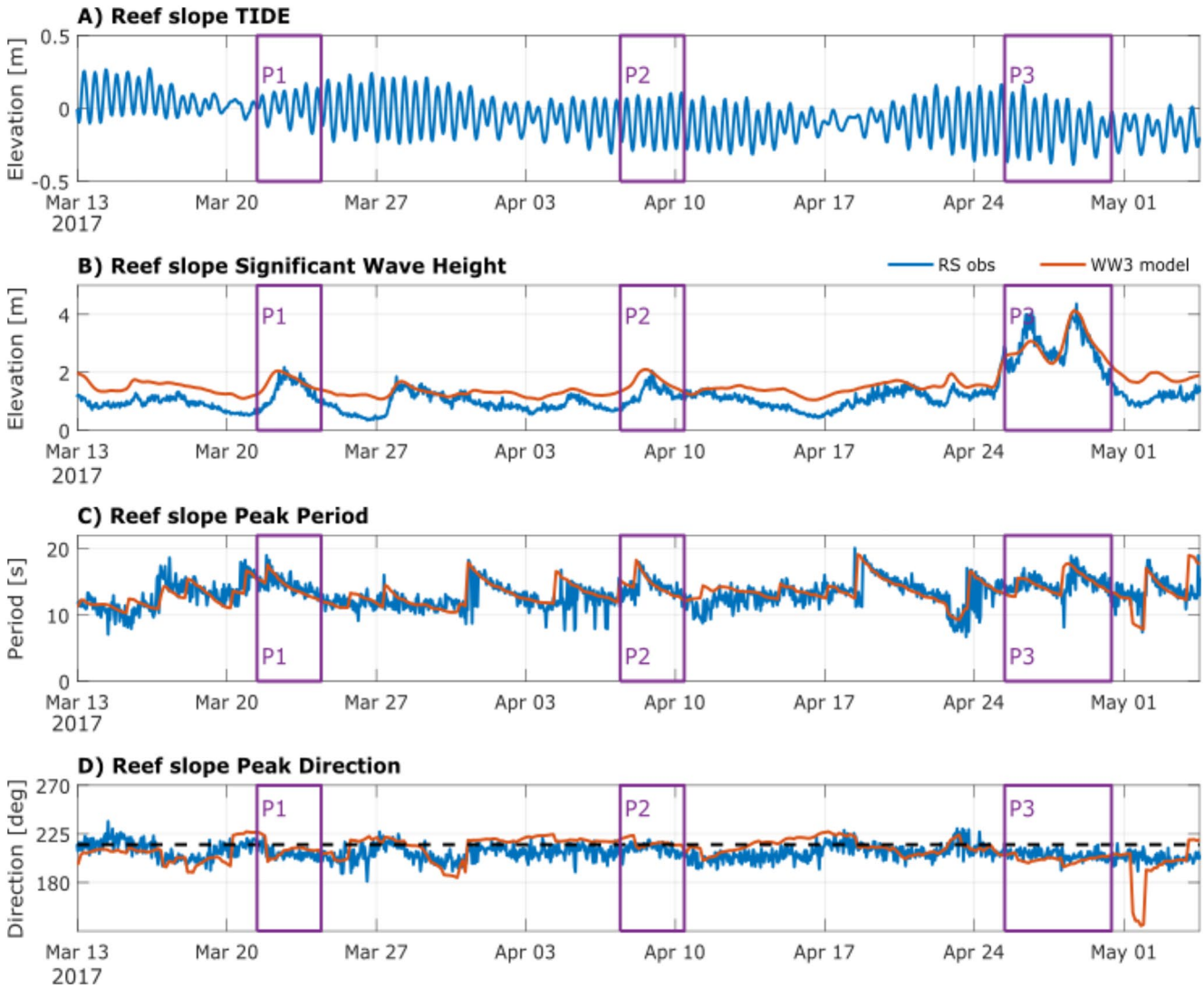

Figure 2. Oceanic forcings during the field experiment. (a) offshore tide measured at the reef slope with the Aquadopp current profiler (AQP), centered on the local datum reference level. (b) significant wave height (H_s). (c) wave peak period (T_p). (d) wave peak direction (θ) clockwise from north. Shore-normal direction is 218° (black dashed line). The WW3 National Centers for Environmental Prediction (NCEP) model data are represented by orange solid lines, and the measured data at the reef slope (RS) in blue. See Figure 1a for the location of the WW3 NCEP model node N1 and the RS station.

wave dynamics and does not account for local wave energy dissipation or shoaling at the shore. The peak wave direction for the local measurements are mainly centered around 220°N which corresponds to the shore normal direction that is around 218° (nautical convention).

Over the whole study period, the low standard deviation of the measured peak direction at the reef slope (std = ±7°) as well as its representativeness of the average conditions during the austral winter allows us to assume that the incoming waves are shore normal. As a result, the reef flat wave measurements are used in the following at the XBeach wave model boundary with a shore normal 1-D numerical domain (cf. Section 3). The differences between the WW3 peak direction and local measurements (Figure 3d) are probably due to local wave refraction processes unaccounted for in the wave model.

The recorded wave conditions are similar to other studies (e.g., Beetham et al. (2016); Cheriton et al. (2016)), with offshore gravity wave significant wave heights reaching 4.3 m, and peak periods reaching 19 s. Three periods of interest were identified corresponding to two moderate swell events marked P1 and P2 and a stronger event marked P3 on Figure 2a. The incident oceanic forcings measured at the reef slope station that allowed to characterize each period are presented in Table 1. Periods P1 and P2 are characterized by a moderate south-south-west

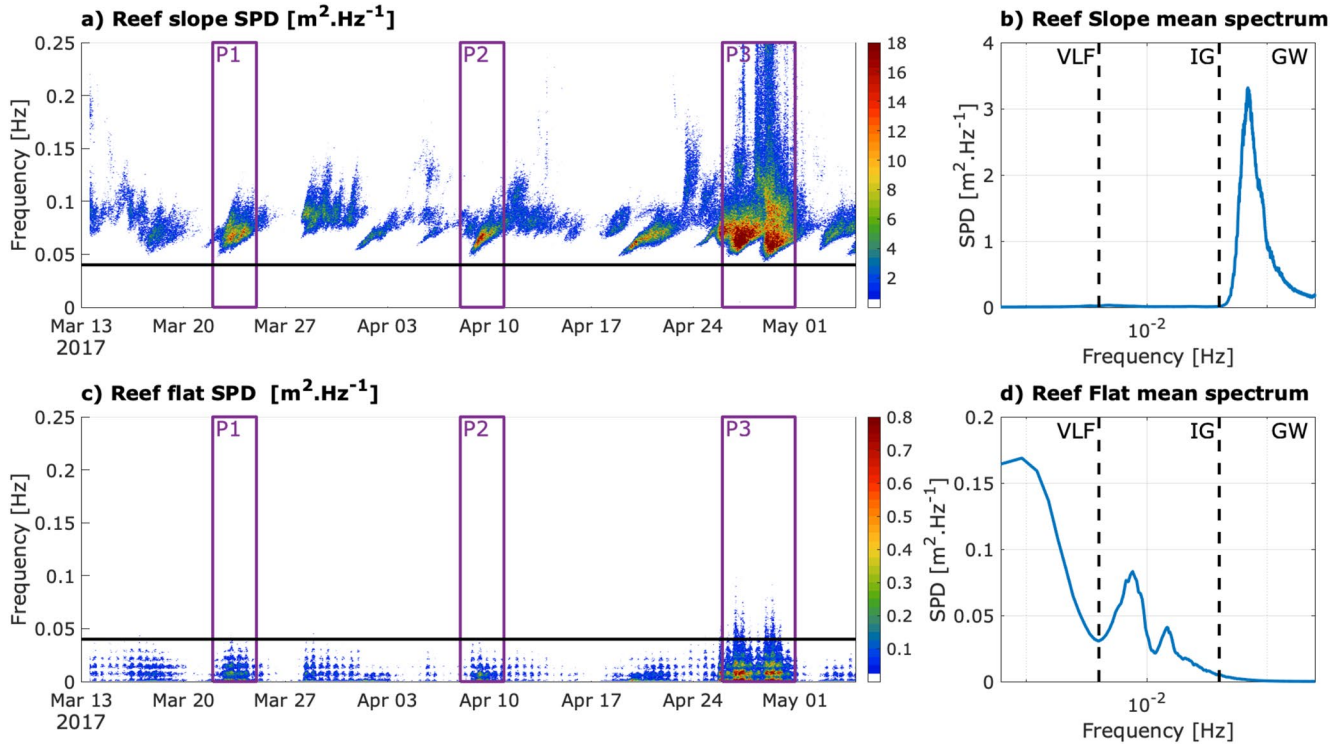

Figure 3. Wave energy spectrum: Temporal evolution at the reef slope (RS) station (a) and at the reef flat (RF) station (c), Total mean wave spectrum over the 53-day of experiment at RS station (b) and at the RF station (d). The black lines represent the frequency bands boundaries (0.04 Hz for IG/GW bands and 0.004 Hz for VLF/IG bands) Periods P1, P2 and P3, corresponding to the wave events of interest, are highlighted by the purple boxes.

swell event with a maximum significant wave height H_S around 2 m and maximum peak period T_P of 19 s P1 and 17.9 s for P2, respectively. The tidal modulations during P1 are relatively weak, characterized by a transition from neap to spring tides, with low mean (21 cm) and full (34 cm) tidal ranges, and a SWL of +0.01 m relative to datum. The tide for the period P2 is characterized by a spring tide with greater MTR (30 cm) and Full Tidal Range (FTR) (40 cm) but a lower SWL (datum −0.09 m). The period P3 is characterized by a strong swell event coming from the south-south-west, occurring at the end of a spring tide (MTR = 34 cm and FTR = 54 cm), with SWL a still water level of datum −0.13. This swell event has two successive peak events with measured significant wave heights of 4.1 and 4.36 m and peak periods of 17.1 and 18.9 s, respectively. These 3 events were selected in the scope of this study because they highlight highly energetic wave conditions under varying tidal and still water levels on a reef system. Neap tides have reduced tidal modulation, and were not considered here.

Table 1
Periods of Interest and Corresponding Offshore Conditions at the Local Measurements RS

Period	Dates	MTR (m)	FTR (m)	SWL (m)	Max (H_s) (m)	Max (T_P) (s)	Mean (D_P) (°)	STD (D_P) (°)
P1	22–24 March	0.21	0.34	0.01	2.17	19	207	±4
P2	08–10 April	0.30	0.40	−0.09	2.04	17.9	211	±5
P3	26–30 April	0.34	0.54	−0.13	4.36	18.9	206	±4

Note. For each period, the Mean Tidal Range (MTR) is the difference between the mean high water and mean low water levels, the Full Tidal Range (FTR) is the difference between the higher and lower water level, the Still Water Level (SWL) is the height of the offshore mean water level relative to the IGN89 datum. The MTR, FTR and SWL are expressed in meters. The wave characteristics are described by the measured maximum values of the significant wave height H_S (m) and peak period T_P (s), and the mean peak direction D_P (°) with its standard deviation.

In the following, the significant wave height H_S is most often used to describe wave height. To simplify the notations providing information of the sample location and the wave frequency band of interest, the signficant wave height is systematic unless specified otherwise (e.g., H_{RMS}). For example, the significant wave height of GW measured at the wave slope is written H_{GW}^{RS}.

3. The Numerical Model

3.1. Model Description

The XBeach model is used to reproduce the physical processes in the La Saline fringing reef and to predict wave runup, which was not measured for this study. Initially developed for mild-sloping sandy beaches (Roelvink et al., 2009), the applicability of the XBeach model in reef environments

and for steep reef bathymetry has been widely tested and validated in the literature (Harris et al., 2018; Pearson et al., 2017; Quataert et al., 2020; Rueda et al., 2019; Storlazzi et al., 2018; van Dongeren et al., 2017). XBeach can be run in short wave-averaged mode (surfbeat) or short wave-resolving mode (non-hydrostatic). The XBeach surfbeat mode (XBSB) resolves the wave energy variations on the wave-group scale which drives IG and VLF long- wave motions but is short-wave averaged (Roelvink et al., 2009). The XBeach non-hydrostatic mode (XBNH) resolves all wave motions and computes the depth-averaged flow due to waves and currents using the nonlinear shallow water equations including a non-hydrostatic pressure correction term (Roelvink et al., 2018).

Here, the model was run in XBSB mode over a 1-D domain with a primary focus on cross-reef wave processes. Using XBSB in 1-D allowed to significantly reduce computational time compared to the XBNH mode, as previously shown by Quataert et al. (2015). Furthermore, a range of studies compare XBNH and XBSB performances, and concur that in shallow-water conditions such as over a fringing reef, both simulation modes provide comparable performances for the prediction of wave setup and extreme runup (Lashley et al., 2018; Quataert et al., 2020). Quataert et al. (2015) also demonstrated that a 1-D XBSB model configuration produced good conservative estimates of the induced IG waves and corresponding runup while considering a shore-normal forcing wave field. Comparison between single-layer models (such as XBSB) and more complex multi-layer models can yield comparable results when in shallow-water conditions (De Ridder et al., 2021). Considering the low directional variability of incident waves observed at the reef slope (std = ±5° over periods P1–3, cf. Figure 2d and Table 1), the wave direction can thus be considered to have negligible impact on cross-reef dynamics, and the incident wave field is then estimated normal to the reef. Consequently, a 1-D XBSB configuration seems suitable to reproduce key cross-shore reef hydrodynamic processes in La Saline reef.

3.2. Model Configuration and Calibration

The bathymetric data set described in Section 2.2 was used as reference data for the XB configuration. The original bathymetric product has a 0.4 m resolution that contains spikes resulting from the complex nature of the reef, which are likely to introduce numerical instabilities. To avoid numerical instabilities, bathymetric errors, and a considerable increase in modeling time, a mesh convergence test was performed. This entailed a comparison of simulation results for a range of different mesh resolutions with the aim of verifying the independence of XB wave transformation (tested for H_{GW}^{RF} and H_{IG}^{RF} especially) from the selected mesh resolution, resulting in the use of a 10 m mesh resolution. The original bathymetry was smoothed using a two-dimensional moving average with a 20 m window size, similar to the coarser grid employed by van Dongeren et al. (2013). The resulting 2-D grid is illustrated in Figure 1b, the cross-shore profile extracted from this grid and used in the 1-D XBSB model is presented in Figure 1c. Since the bathymetric product focused only on the submerged part of the fringing reef, and to avoid overtopping up to the model land boundary, the topography of the beach face was artificially prolonged considering a beach slope of 1:10 up to 5 m above the IGN89 datum (highest vertical location of the beach profile) in correspondence with beach profiles available for this area (data not shown, cf., Mahabot et al. (2017)). The hourly averaged tidal water levels and the wave variance density spectra computed using the reef slope OSSI pressure sensor measurements are used to force the XBeach model at its offshore boundary. The tidal variations were applied over the entire domain, while the incident gravity wave spectra were applied at the offshore boundary with frequencies ranging from 0 to 0.25 Hz using a 1.5×10^{-3} Hz discretization, and a 40° spectral directional spread. A one-dimensional absorbing-generating weakly reflective condition was applied at the offshore and land boundaries.

A critical step in modeling reef hydrodynamics is the parameterization of depth-driven wave energy dissipation. In the XBSB mode, dissipation is parameterized with a gravity wave friction coefficient f_w and the bottom friction coefficient c_f associated with mean currents and low frequency wave-induced motions. The estimation of f_w and c_f is a challenge in rough reef environments, and have been the focus of many studies. The short-wave friction coefficient f_w appears as a factor of key importance for the assessment of the wave energy dissipation, with Harris et al. (2018) directly linking this factor to the cover of living corals and the structural complexity of the coral reefs. f_w is thought to be at least an order of magnitude greater than c_f (Lowe et al., 2007). A number of theoretical and empirical values of f_w have been proposed in the literature, often ranging between $f_w = 0.1$ and $f_w = 0.5$, with increasing friction for increasing coral complexity (Harris et al., 2018; Lentz et al., 2016), and sometimes reaching exceptionally high values such as $f_w = 1.8$ in a north Pacific atoll (Monismith et al., 2015) or even $f_w = 5.0$ on coral reef platforms in the Red Sea (Lentz et al., 2016).

In the present study, the gravity wave friction and the bed friction coefficients were calibrated so that the best match was found between the simulated XBeach wave parameters and setup over the reef flat and the field measurements, for the widest possible range of conditions. The optimal values for the configuration of the XBeach model were found to be $f_w = 0.3$ and a depth-dependent Manning formulation $c_f = \frac{gn^2}{h^{1/3}}$ with $n = 0.02$, g the gravity constant, and h the water level. This leads to spatially and time varying c_f-values spanning 0.005–0.02 at the reef crest. Gravity wave dissipation through breaking is an essential mechanism, and best modeling results were obtained using the breaking formulation proposed by Roelvink and Brøker (1993) with which wave dissipation is proportional to H^2. The wave dissipation coefficient α and the breaker index γ are set to default model values ($\alpha = 1.0$ and $\gamma = 0.55$).

3.3. Data Processing and Model Validation

The XB wave-induced setup, the IG and VLF wave heights were calculated using the same methods as used for the observed data and described in Section 2.2 (cf. Equation 1 for setup and spectral analysis). Subsequently, the model results were post-processed to compute 10-min water levels and root-mean-square wave heights H_{RMS} for GW, IG and VLF waves, at RS and RF instrument locations. Also using 10-min segments, the setup was estimated from difference between RF and RS water levels. Finally, the modeled significant wave heights H_S were deduced from H_{RMS} according to the equation $H_S = \sqrt{2}H_{RMS}$ considered valid when assuming Rayleigh-distributed wave heights.

To qualify the accuracy of the model configuration, we used the observed setup and significant GW, IG and VLF wave heights at the reef flat station, and computed three statistical parameters, the coefficient of determination R^2, the RMSE and the *Bias*:

$$R^2 = 1 - \frac{\sum_{i=1}^{n}(O_i - P_i)^2}{\sum_{i=1}^{n}\left(O_i - \underline{O}\right)^2} \tag{3}$$

$$RMSE = \sqrt{\frac{1}{n}\sum_{i=1}^{n}(O_i - P_i)^2} \tag{4}$$

$$Bias = \sum_{i=1}^{n}\frac{(O_i - P_i)}{n} \tag{5}$$

where P_i and O_i are the *ith* predicted and observed data respectively, $\underline{O}$ denotes the temporal mean of the observed data, and n is the total number of measurements.

The wave runup was computed by the numerical model at 1 Hz output frequency over the entire study period. The runup was obtained through the detection of the waterline height (m), from which the tidal contribution was removed. For coherence with data analysis methods presented in Section 2.2, and the frequency of forcings applied at the XB offshore boundary, 10 min runup averages were calculated. In the following, the presented runup is the top 2% of the runup modeled with XB (sometimes referred to as *R2%* in the scientific community). With the present study XB model configuration, runup is mainly associated with the longer waves that are fully resolved in the XBSB mode. This assumption holds if there is high short wave energy dissipation of over the reef flat in most reef systems.

4. Results

4.1. Wave Spectra Observations

The wave spectra for the 53-day observations on the reef slope and the reef flat are illustrated in Figure 3. The left panel of the plot shows the time series of observed power spectral densities, whilst the right panel shows the spectra temporal means over the study period, with black dashed lines at 0.004 and 0.04 Hz, highlighting the boundaries between the VLF, IG and GW frequency bands. The three periods of interest P1, P2 and P3 are also

indicated by purple boxes. First, the temporally averaged spectra (Figures 3b and 3d) shows that the limit that was fixed between the GW-IG bands (limit at 0.04 Hz) and the IG-VLF bands (limit at 0.004 Hz) appears to be a good choice in our study since the average spectrum reveals a local minimum of energy at these frequencies.

The GW are almost totally dissipated while the waves break and propagate across the reef, characterized by a strong reduction of the spectral power density between RS and RF (Figures 3a and 3c). The reef clearly acts as a low-pass filter maintaining energy in the IG band on the reef flat. Over the entire study period, the presence of a double peak in the IG band is observed, as also observed during specific events, with a first peak at 0.0076 Hz (≈2 min) and a second peak at 0.0150 Hz (≈1 min), possibly implying harmonic behavior. On the reef flat (Figure 3d), the maximum of energy in VLF band is more than twice the maximum of energy in the IG band, with a large peak of energy at 9.10^{-4} Hz (≈18.5 min). This value is of the same order of magnitude to the first seiche mode period of 15 min, considering the first seiche mode period as $\frac{4L}{\sqrt{gh}}$ with $L = 500$ m, the width of the reef, and $h = 0.5$ m, the mean reef water depth. On the reef flat, the level of IG and VLF energy is higher during extreme events (Figure 3c) suggesting that the GW energy is the forcing mechanism. As a result of the high proportion of wave energy in the GW range at the RS, the energy in the VLF and IG are comparatively dwarfed (cf. Figure 3b). Contrary to appearances, the energy at the RF and RS in the VLF and IG ranges remain comparable, with a factor 1.5 between RF and RS H_{IG} (cf. Section 4.2.1).

4.2. Wave and Water Level Observations

4.2.1. Water Levels

Figure 4 shows the time series of the water level and wave parameters measured at the reef slope and reef flat stations. The observed tide was similar to the one described in Figure 2a, mainly semi-diurnal with a diurnal inequality, covering two neap tides and two spring tides. The tidal range was almost similar in the reef slope and in the reef flat, around 0.5 m for the two spring tides and 0.2 m for the two neap tides. The maximum high tide was +0.23 m and the minimum low tide −0.24 m for the first spring tide, respectively +0.19 m and −0.35 m for the second spring tide. For the first neap tide, the maximum high and minimum low tides were 0.08 m above and below datum respectively, for the second neap tides the maximum was +0.01 m and the minimum was −0.20 m (Figure 4a).

4.2.2. Short and Long Waves in the Reef

The reef slope GW significant wave height H_{GW}^{RS} was 1.4 m on average, with mean and maximum spectral energetic period $T_{m0,-1}$ of 10.9 and 15.8 s respectively (Figures 4b and 4c). For the two swell events of the periods P1 and P2, H_{GW}^{RS} reached ≈2 m with periods $T_{m0,-1} = 13.9$ s during P1 and 14.5 s during P2. The stronger swell event P3 that occurred at the end of April was a double peaked swells with a first event $H_{GW}^{RS} = 4.2$ m and $T_{m0,-1} = 13.6$ s, and a second event characterized by higher wave heights ($H_{GW}^{RS} = 4.7$ m) and lower periods ($T_{m0,-1} = 11.7$ s). In the reef flat, during P1 and P2 events, the significant GW heights did not exceed 10 cm, but reached 20 cm during P3, demonstrating the marked attenuation of short wave components by the reef. This GW attenuation across the reef flat is evident with a 97% mean reduction of the incident wave heights (Figure 5a), and an observed H_{GW}^{RS} of 0.04 m on average (cf. Figure 4c). Wave attenuation varied between 92% and 98% from high tide to low tide respectively, suggesting that the tidal fluctuations partially controlled the gravity wave energy reduction, with a lower attenuation of incident waves during high tide, and greater attenuation during low tide (Figure 5a).

The transformation of the waves while they propagate across the reef is clearly evident with spectral analysis (Figure 3) through the filtering of the high-frequency, related to the dissipation of the shorter frequencies due to breaking and bottom friction and an energy transfer to lower frequencies. On the reef flat observations, the simultaneous increase of the lower frequency wave heights and decrease of the GW confirmed this process (Figures 4d, 4e, 4g, & 4i). Over the entire studied period, the synchronicity between the long wave variability on the reef flat (IG and VLF wave heights in Figures 4d and 4e) and the reef slope GW (Figure 4c), suggests that the lower frequency waves that appeared in the reef flat were primarily controlled by the incident swells.

The IG wave heights in the reef flat ranged from 1% to 12% of the incident oceanic gravity wave conditions (Figure 5b) and were on average 1.5 times greater than the IG waves observed on the reef slope ($H_{IG}^{RF} = 9.4$ cm and $H_{IG}^{RS} = 6.2$ cm). This ratio was clearly modulated by tide, increasing with the water level on the reef, but this

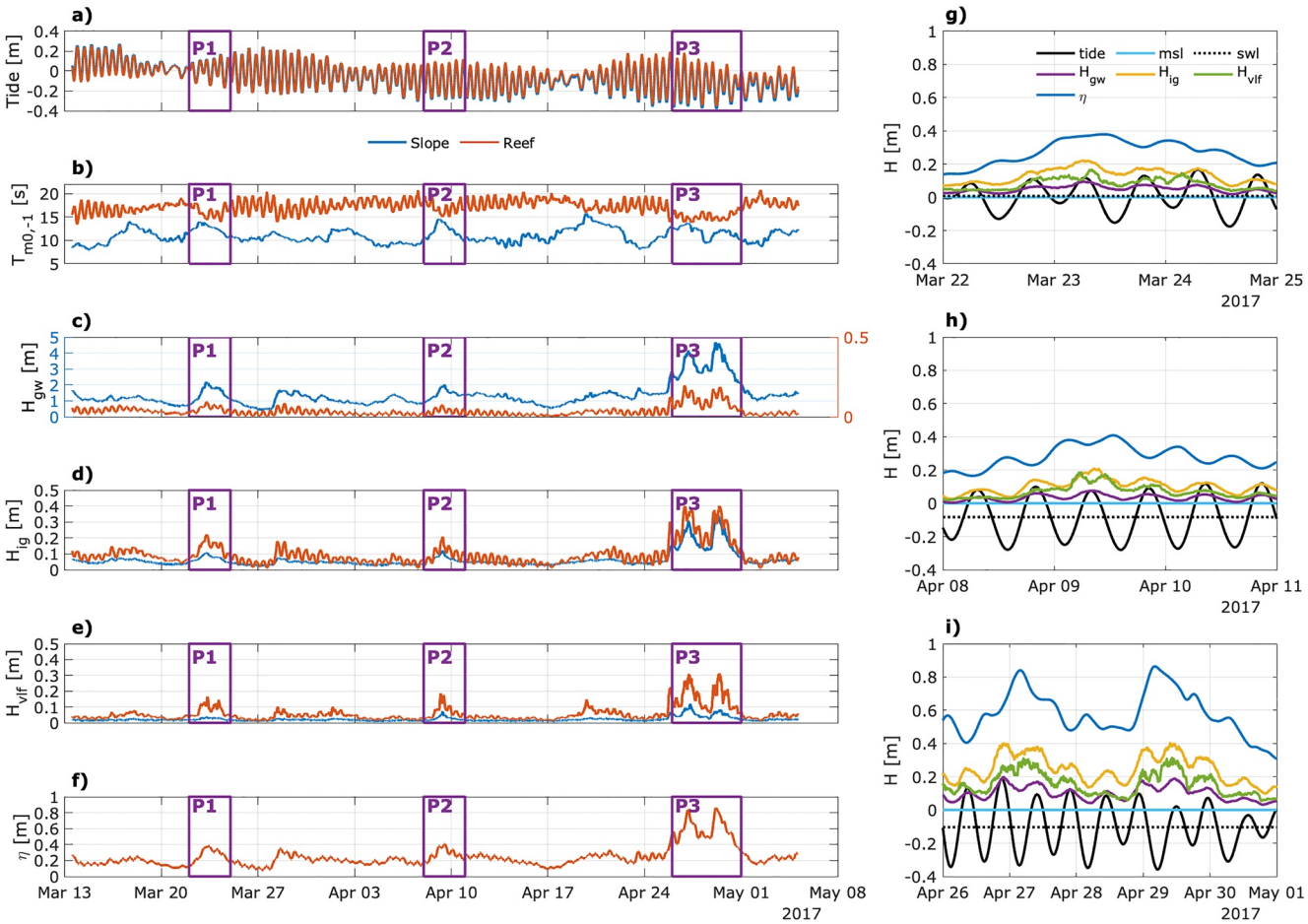

Figure 4. Overview of hydrodynamic measurements. On the left hand side, the water levels and wave parameters for the reef slope (in blue) and the reef flat (RF) (in red) observations over the 53-day of deployment: (a) Tide (relative to IGN89 datum) (b) Mean spectral period (c–e) Significant wave heights in the gravity waves (GW) band H_{GW}, gravity waves (GW) band H_{IG}, and VLF band H_{VLF}. (f) Setup η computed at the RF station. On the right hand side, zoom on: (g) P1, (h) P2 and (i) P3 periods for the RF parameters. Each zoom is illustrated with the tide (black line), the level of reference (blue horizontal line at 0 m), the still water level (SWL, black dotted line), as well as H_{GW}, H_{IG}, H_{VLF}, and setup (shown with orange, yellow, green and blue curves, respectively).

tidal modulation behaved differently above an incident GW height threshold $H_{GW}^{RS} = 2.5$ m and was reduced to a quasi-constant ratio value (Figure 5b), suggesting that the reef flat IG waves became primarily controlled by incident short waves rather than tides. The tidal modulation of the reef flat IG wave heights is also evidenced by an oscillating component of these IG waves in phase with tidal signal (Figures 4g–4i), increasing with the rising tide (Figure 5d). While focusing on the three periods of interest, for which the MTR increases from P1 to P3 (cf. Table 1), the amplitude of the tidal modulation appeared more pronounced for stronger tidal range (Figures 4g–4i). The amplitude of IG wave reaches up to 40 cm during P3.

Similarly, VLF wave heights on the reef flat were enhanced by a factor of 2.6 on average, between the reef slope and the reef flat, corresponding to mean wave height $H_{VLF}^{RF} = 5.6$ cm on the reef flat and $H_{VLF}^{RS} = 2.1$ cm on the reef slope. The ratio between VLF wave height in the reef flat and GW on the reef slope ranged from 1% to 10% (4% on average) with very slight modulations at a tidal scale, less pronounced during energetic events (Figures 4g–4i and Figures 5c and 5e). During P3, VLF significant wave height reaches 30 cm.

4.2.3. Wave Friction Factor Estimation on the Reef

In order to reproduce the variability of the GW on the reef flat H_{GW}^{RF}, wave dissipation due to breaking and the bottom wave friction must be considered. We used the analytic expression for the wave height decay onshore of

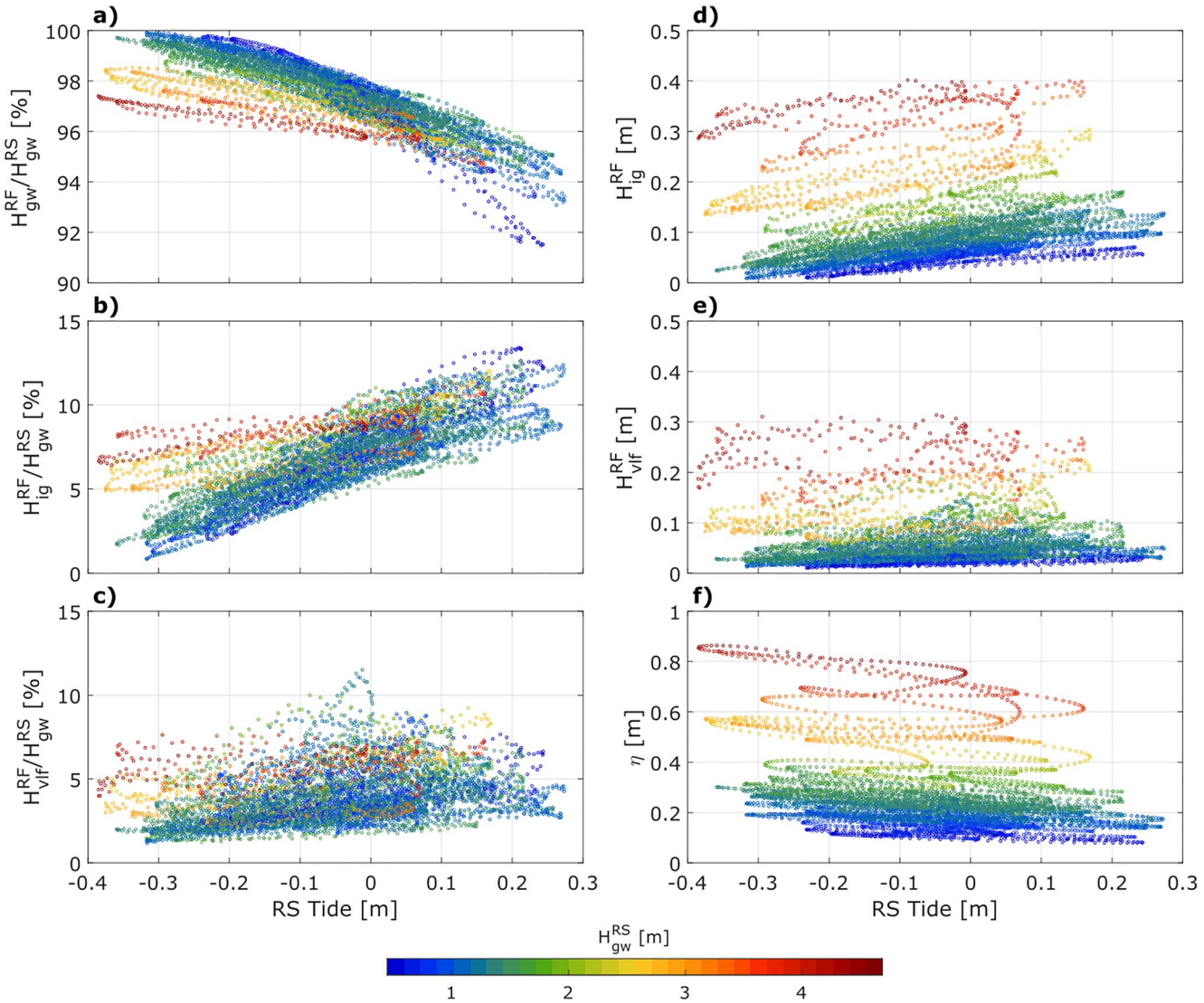

Figure 5. Tidal control on wave processes in the reef flat (RF): (a) gravity waves (GW) attenuation, (b–c) ratio between the low frequency waves (gravity waves (GW) and VLF) of the RF and reef slope (RS) GW, (d–e) IG and VLF wave heights, (f) setup at RF station. All scatter plots are colored by the height of the reef slope GW.

the surf zone (Lentz et al., 2016), assuming a constant water depth, the wave friction factor f_w and shallow water waves (Equation 6):

$$H^{RF}_{GW}(L) = \gamma \frac{D+\eta}{1+\frac{L}{L_d}} \tag{6}$$

In this equation, L is the distance separating the measurement location and the reef crest, D is the water depth and η the setup, γ is the breaker index equal to the wave height to water depth ratio at the onshore edge of the surf zone, and $L_d = 8\sqrt{2\pi}\frac{D+\eta}{\gamma f_w}$ is a frictional decay scale in which f_w is the wave friction factor. We note that in this equation, in the absence of frictional wave dissipation ($f_w = 0$) the gravity wave height is directly related to the water depth by the breaker index $H_{GW} = \gamma(D+\eta)$, as expected.

To accurately reproduce the dependence of wave height on water depth in the reef flat, the two parameters f_w and γ must be correctly chosen. In absence of observations in the breaking zone to quantify wave height and water depth, the breaker index was set to $\gamma = 0.55$ equal to the default value used in the XBeach model (cf. Section 3.2 on model configuration). The wave height variability described by Equation 6 is well-reproduced for a wave

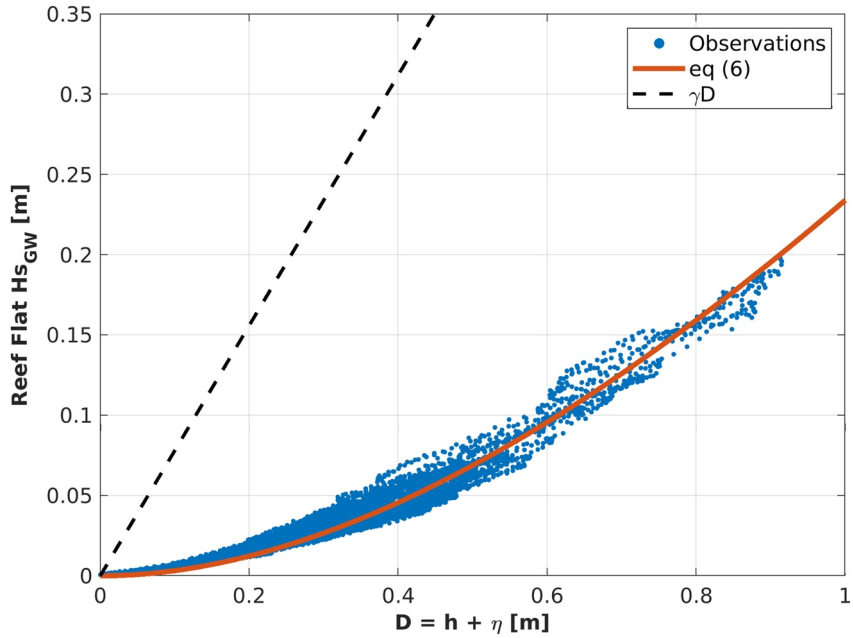

Figure 6. GW height at reef flat (RF) station according to the modified depth above the reef crest following the adapted Lentz et al. (2016) equation (Equation 6).

friction parameter $f_w = 0.2$ (orange solid line, Figure 6), reinforcing the assumption that the bottom friction plays a key role in the relationship between wave height and water depth on the reef flat after the breaking zone. When bottom drag dissipation is large, the ratio H_s/D is not representative of the value of the ratio γ in the surf zone, illustrated by the black dashed line in Figure 6. We note that this $f_w = 0.2$ value is lower than the $f_w = 0.3$ found for the configuration of XBeach (cf. Section 3.2).

4.2.4. Setup

Wave setup on the reef ranged from 0.08 m (12% of incident H_{GW}^{RS}) to 0.86 m (18% of H_{GW}^{RS}) with a mean value of 0.25 m, representing 18% of the incident offshore mean wave height. Considering the strong correlation coefficient obtained for Equation 2 ($R^2 = 0.95$), the setup in the reef is highly correlated to the incident wave height. Meanwhile, for similar incident conditions, the setup is slightly lower at high tide and higher at low tide (Figure 5f). The setup variations are in antiphase with the tidal signal (blue curve in Figures 4g–4i). The maximum observed setup is 0.86 m during the extreme event P3 corresponding to incident wave height $H_{GW}^{RS} = 4.7$ m and energetic period $T_{m0,-1} = 11.7$ s and a tide level −0.36 m relative to IGN89 datum. Similarly to IG and VLF waves, setup increases more rapidly for incident waves above 2.5 m in significant wave height.

4.3. Model Results

4.3.1. Model Validation

A comparison of the measured and modeled wave characteristics across the fringing reef is presented in Figure 7. High correlations indicate that the model configuration is well adapted the prediction of H_{GW}^{RF}, H_{IG}^{RF} and setup over the reef.

Since the model was forced by variance density spectra computed from measurements, the good correlation (with $R^2 = 0.99$) between modeled and measured GW at the reef slope $\left(H_{GW}^{RS}\right)$ is expected (Figure 7a). However, modeled wave heights seemed to be slightly underestimated for the strong swell event P3 (Figure 7f). At the reef flat, the model performance is good with $R^2 > 0.88$, $Bias < 0.033$ m and $RMSE < 0.046$ m based on the output H_{GW}^{RF}, H_{IG}^{RF}, and setup on the reef flat (Figures 7b, 7c and 7e). The GW in the reef flat are well-represented during the P1 period, but overestimated for P2 and P3 periods for observed $H_{GW}^{RF} < 0.12$ m in the reef flat and underestimated for $H_{GW}^{RF} > 0.12$ m (Figure 7g). Despite good performance metrics of the model for IG waves in the reef flat, they are generally underestimated during the three periods of interest (Figure 7h). The model behaves

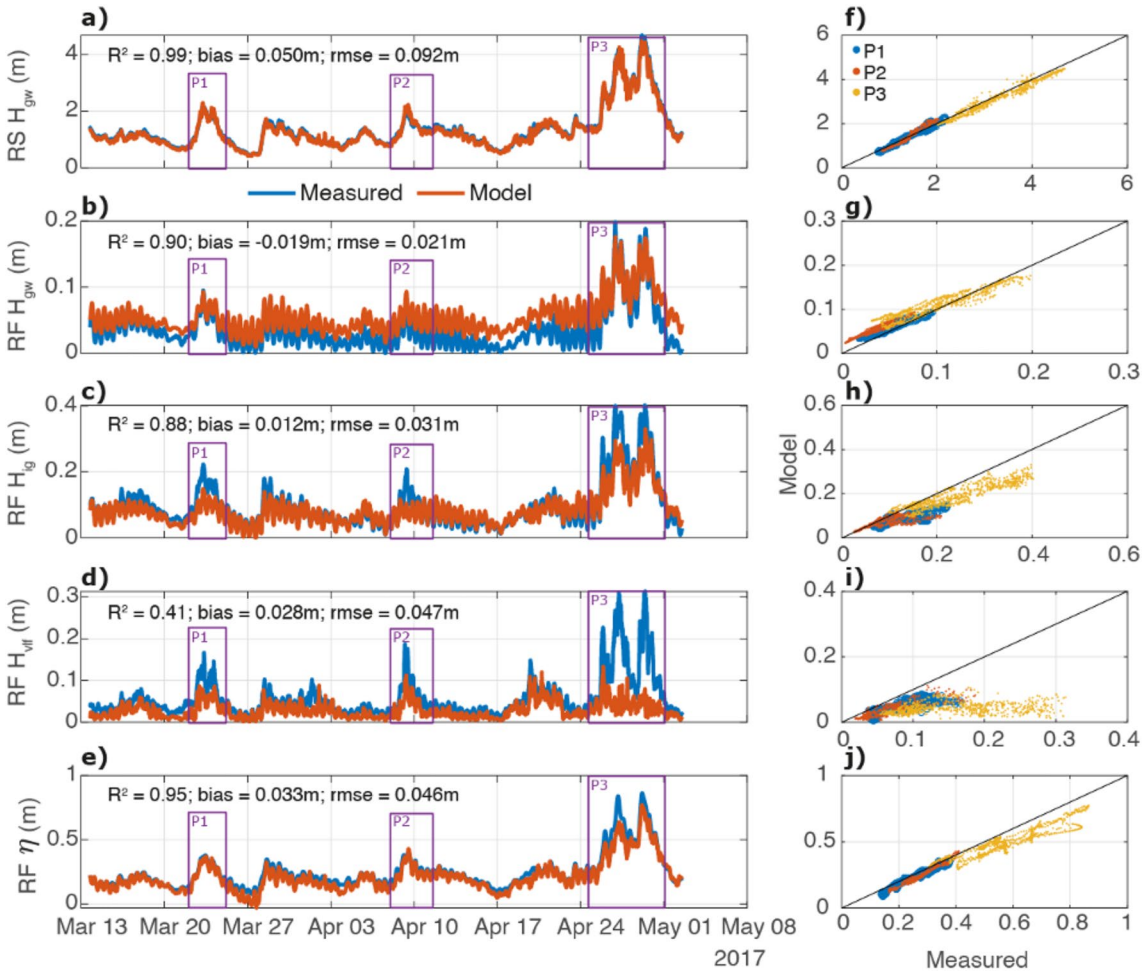

Figure 7. Comparison of measured and modeled reef hydrodynamics. Left hand side panels: timeseries of the modeled (in red) and observed (in blue) wave parameters on (a) the reef slope, (b–d) the reef flat (RF) and (e) setup on the RF. The performance metrics of the model over the whole period that are R^2, the *Bias* and the *RMSE*, are also indicated. Right hand side panels: scatter plots of measured versus modeled parameters for the three periods of interest, P1 in blue, P2 in red and P3 in yellow.

especially well for the prediction of the setup, with a slight underestimation in the reef flat for values greater than 0.4 m during the P3 period (Figures 7e and 7j). Figure 8 allows a focus on the measured and XBeach modeled setup over the three study periods P1–3. Whilst setup increases with the H_{GW}^{RS} at the reef slope, the effects of the tidal oscillations on the setup is well reproduced by the XBeach model (e.g., Figure 8b). For the P3 period, the *Bias* between the measured and the modeled setup increases and reaches 10 cm.

The VLF wave heights, however, were poorly reproduced by the model, with a weak $R^2 = 0.41$ for the whole period and a clear underestimation over the three periods of interest. VLF variability is numerically captured overall, with the exception of P3 (cf. Figure 7d).

4.3.2. Modeled Runup

Following comparison with field data (cf. Section 4.3.2), the XBeach model is used to estimate runup. Figure 8 presents the XBeach-modeled runup over the three study periods P1–3. The modeled runup is globally 10 cm higher than the setup during P1 and P2, and reaches extreme values during P3, reaching 1 m, up to 40 cm higher than the modeled setup during the first peak of the P3 event (Figure 8c).

The relative contributions of other parameters to the water level at the shoreline (combination of wave runup and tidal fluctuations) are also investigated, and presented in Table 2. The offshore tide level is shown to contribute to about 19% over the whole period, and also during extreme events. The setup contributes to the most important part of the water level, by approximately 68% for the whole period, 67% for P1 and P2, and 61% for P3. The main

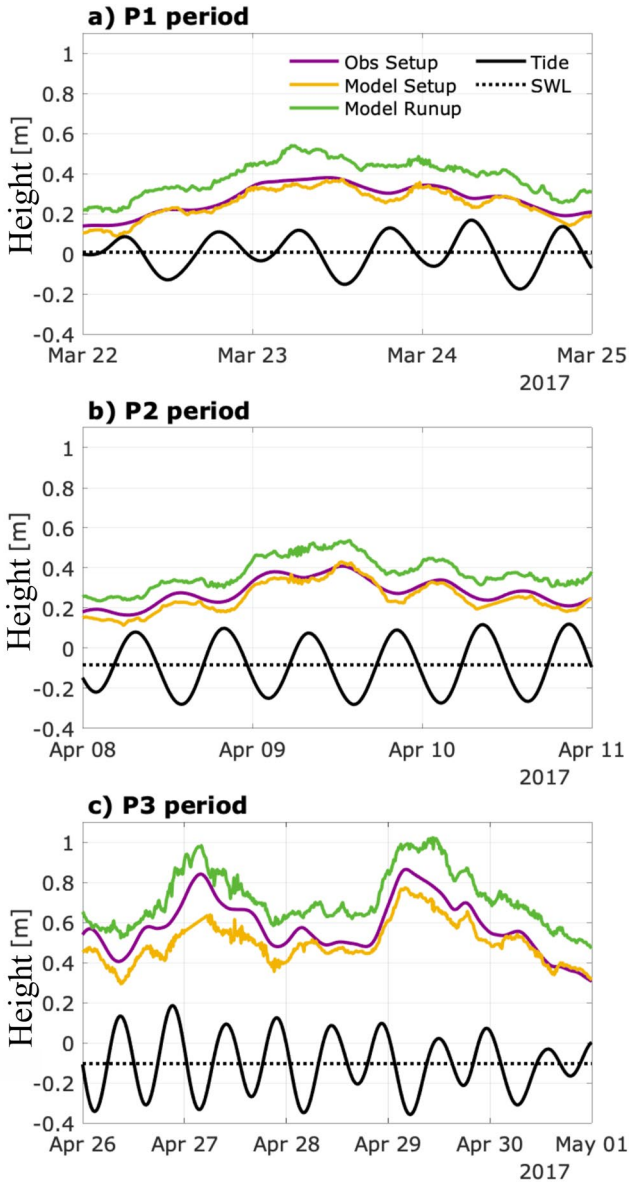

Figure 8. Observed and simulated elevations during (a) P1, (b) P2 and (c) P3 events: setup height (m) over the reef flat (RF) computed from observations (purple line), modeled setup (yellow line), modeled wave runup at the beach (green line), observed tide (black line) and still water level (dashed black line).

differences lie in the contribution of the GW on the reef flat, which contribute to 1% of the water level at the shoreline for the P1 and P2 events, and more than 7% during the P3 event. The longer waves (IG and VLF) equally explain 5%–7% of the water level for all the periods, with an exception of the IG waves which account for 10% of the water level at the shoreline during the P1 period. The relative importance of each variable reinforces the assessment that each of these parameters must therefore be correctly predicted according to offshore water level and energy in order to correctly quantify the evolution and variability of the water level at the shoreline.

4.4. Transfer Functions

Transfer functions (using multiple linear regressions) are fitted between incident conditions (offshore water level and wave parameters) and reef flat parameters (H_{GW}^{RF}, H_{IG}^{RF}, H_{VLF}^{RF}, setup and runup) in order to be able to predict the runup in the context of global change. Several parameters are considered: the offshore water level relative to the reef crest D, the distance to the reef crest L, the GW significant wave height and period at the RS station, wave energy, wave power, or even $H_S T_m^2$ (Ardhuin et al., 2014). The best fits and correlation statistics are presented in Figure 9 and Table 3. Figure 9 highlights the dependency of RS H_{VLF}^{RS} and H_{IG}^{RS} to the incident wave power ($R^2 = 0.83$ and 0.97 respectively) and of the RF H_{VLF}^{RF} and H_{IG}^{RF} to significant wave height, water level and incident wave power ($R^2 = 0.85$ and 0.95 respectively). The statistical parameters and best fit equations are summarized in Table 3, considering $P = H_{GW}^2 \times T_{m0,-1}$, where P is proportional to the wave power. These transfer functions highlight the fact that the forcing mechanism is oceanic swell. The water level at the RF is shown to positively influence the H_{VLF}^{RF} and H_{IG}^{RF} by 4% and 12%, respectively.

A transfer function reaching $R^2 = 0.97$ with a standard deviation of 2 cm is found for the setup using the RS GW height and the water level (Table 3 and Figure 9c). 98% of setup is explained by incident wave conditions. The water level negatively influences the setup and is responsible for 2% of its variability. Furthermore, 79% of the runup is explained by incident wave conditions and 21% by tidal fluctuations. Combining both forcings leads to $R^2 = 0.94$ with a RMSE of 4 cm (Figure 9f and Table 3). The higher the offshore water level, higher the runup at the shoreline.

5. Discussion

The objective of this study is to provide a better understanding of the coastal defense capabilities of the fringing La Saline reef system at la Réunion Island as a function of the incident wave field and tidal characteristics. Over the 53-day study period the study site was exposed to a range of energetic swell events generated in the Southern Ocean. Field data was collected at the reef slope and the reef flat. These field observations were used to calibrate and validate the XBeach numerical model, allowing further investigation of wave transformation processes, setup and runup in the reef system.

5.1. Gravity Wave Driven Hydrodynamics

Measurements allowed to identify GW, IG waves, and VLF waves on the reef flat, as previously reported in similar environments (e.g., Bonneton et al., 2007; Ferrario et al., 2014; van Dongeren et al., 2017; Pearson et al., 2017). The study of IG and VLF wave magnitudes demonstrates that the lower frequency components

Table 2
Relative Contributions of the Tide at the Reef Slope, Setup, GW, IG and VLF at the Reef Flat to the Water Level at the Shoreline During (From Left to Right) the Whole Period, Periods P1, P2 and P3

Relative contribution to water level at shoreline (%)	Whole period	P1	P2	P3
Tide	18.95%	16.22%	17.62%	17.36%
Setup	67.88%	66.59%	66.9%	61.4%
GW	3.55%	1.06%	0.97%	7.46%
IG	5.52%	9.83%	7.47%	7.24%
VLF	4.1%	6.30%	7.04%	6.55%

observed at the reef slope and reef flat are strongly in phase with incident GW swell conditions (Figures 4, 5 and 7 and Table 3), confirming that waves sourced from the open ocean are the main driver of the reef system hydrodynamics. This is in line with similar findings at other reefs (e.g., Beetham et al., 2016).

5.2. Wave Dissipation

Coral reefs offer substantial protection against natural hazards (e.g., Ferrario et al., 2014; van Dongeren et al., 2017). The coastal defense abilities of La Saline fringing reef are first confirmed by the average reduction of 97% of GW energy over the whole measurement period (cf. Section 4.2.2). While most of the energy reduction occurs at the reef crest (Ferrario et al., 2014; Monismith et al., 2015; Vetter et al., 2010), bottom friction contributes to wave dissipation of waves propagating over the reef flat canopy (Symonds et al., 1995). The friction factor f_w varies considerably between study sites (Harris et al., 2018; Lowe et al., 2005; Rogers et al., 2016).

To estimate f_w in La Saline reef, one approach is to use the depth-dependent analytical model (cf. Equation 6) introduced by Lentz et al. (2016) for fringing reefs. The best fit of this formulation to our field measurements is found for an average value of $f_w = 0.2$ (cf. Figure 6) for the entirety of the campaign, considering a breaker index $\gamma = 0.55$ similar to the default value in the XBeach model. This inferred friction factor is within the range of values reported by authors such as 0.3 at the Kanehoe barrier reef (Lowe et al., 2005), and 0.2 at Moorea's north shore fringing reef (Monismith et al., 2013), though $f_w = 0.2$ remains low friction factor for coral reefs. With such a value, this friction factor leads to a wave decay close to 40% more intense than when considering wave breaking only (compare black line and orange line for a fixed water level value in Figure 6). Such results are dependent on factors such a reef health and water level, which are both expected to evolve with predicted environmental change (IPCC report – Hoegh-Guldberg et al. (2014)).

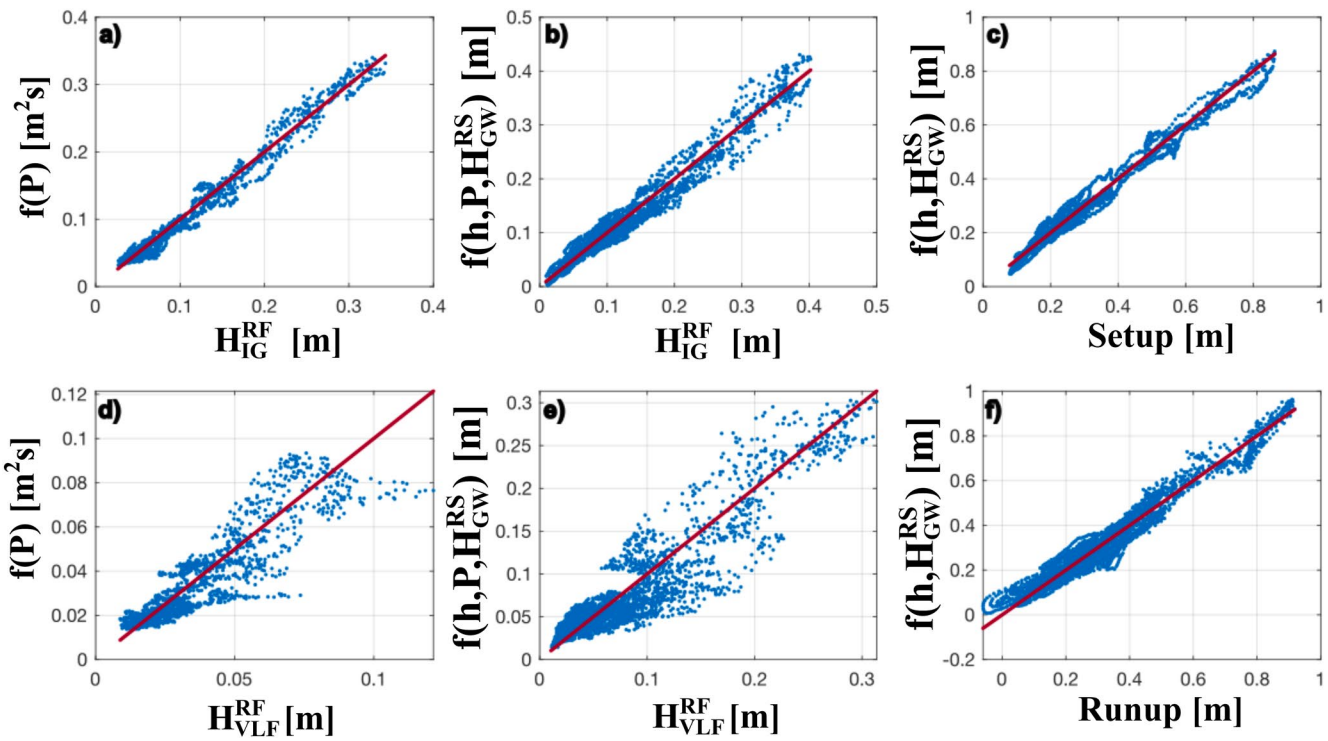

Figure 9. Best fit functions (see transfer functions in Table 3) for the prediction of (a) reef slope (RS) gravity waves (GW) wave height, (b) reef flat (RF) IG wave height, (c) Setup, (d) RS VLF wave height, (e) RF VLF wave height, and (f) Runup. Red lines represent identity. Correlation statistics for the above relations are presented in Table 3.

Table 3
Transfer Function, Best Fit Function According to Multilinear Regression, for 6 Variables (Cf. Figure 9) With the Associated R^2, RMSE and the Ratio of Explained Variability by Each Individual Parameter

Parameter	Transfer function	R^2	*RMSE*	Predicted %var		
				RS tide	H_{GW}^{RS}	RS *P*
H_{IG}^{RS}	$0.0012P + 0.03$ (7)	0.97	0.9 cm	-	-	99.9%
H_{VLF}^{RS}	$0.0003P + 0.013$ (8)	0.83	0.6 cm	-	-	99.9%
H_{IG}^{RF}	$0.187\ h + 0.045\ H_{GW}^{RS} + 0.0009P + 0.021$ (9)	0.95	1.5 cm	12%	86%	2%
H_{VLF}^{RF}	$0.07\ h + 0.004\ H_{GW}^{RS} + 0.001P + 0.026$ (10)	0.85	1.9 cm	4%	89%	7%
RF Setup	$0.176\ H_{GW}^{RS}$ - $0.144\ h$ (11)	0.97	2.3 cm	2%	98%	-
RF Runup	$0.210 H_{GW}^{RS} + 0.593\ h + 0.041$ (12)	0.94	4.1 cm	21%	79%	-

Note. Six transfer functions are proposed and become Equations 7–12 of this study. *P* is the wave power, *h* is the water level.

The analytical model (Lentz et al., 2016) is validated in the case of the La Saline fringing reef (cf. Figure 6). These results illustrate the importance of bottom friction and water level on the wave decay across the reef flat. Indeed, higher water levels lead to reduced dissipation due to wave breaking and bed friction dissipation (e.g., Figure 5a). We note that in the case of the platform coral reef configuration studied by Lentz et al. (2016), it is not clear if setup plays a major role in GW height over the reef flat. We highlight that over a fringing reef such as La Saline, the setup (of a few dozen centimeters) is of the same order of magnitude as the water depth below the still water level (cf. Figures 4 and 8). Setup is an essential and even dominant component in calculations of wave dissipation (cf. Figure 9). As setup over the reef flat decreases, so does the bed friction dissipation as the total water depth is increased. As it becomes clear that the total water depth on the reef flat (including the setup) must be reported at the breaking location (at the reef crest), the correction (by subtraction) of the generally higher level found at the reef crest is necessary, with the aim of attaining $D = 0$ in conditions of absent waves at the reef crest (H_{GW}^{RF} at RF station). Whereas in Lentz et al. (2016), much data was in the linear part of the model (cf. Equation 6), the present study completes the validation, by adding much data in the polynomial section of the curve, at low water levels (cf. Figure 6).

5.3. Wave Transformation

As the gravity wave components are dissipated over the reef, lower frequency waves are amplified (i.e., IG and VLF waves). Pressure sensor data show that IG and VLF components represent 7% and 4% of the total incident wave energy, but experience an average 150% increase in H_{IG}^{RF}, and a 260% increase in H_{VLF}^{RF} over the reef flat. These observations demonstrate the low-pass filtering capacity of the reef, already evidenced in a number of studies (Beetham et al., 2016; Cheriton et al., 2016; Péquignet et al., 2014; Pomeroy et al., 2012, 2015; van Dongeren et al., 2013). For the lower frequency wave components, we find that VLF and IG waves height at the RS station are linearly related to incident wave power (Figure 9 and Table 3). In addition to being strongly related to wave height (86% of variance explained by offshore wave heights, cf. Table 3), IG wave height on the reef flat is also strongly modulated by the water level (12% of variance). Since the breaking is modulated by the depth, this would explain the influence of the depth on the IG wave height at RF station. IG wave energy that is not dissipated over the reef flat may be reflected seaward, and might lead to resonant VLF waves (Bertin et al., 2018; Gawehn et al., 2016). This would explain the fact that the H_{VLF}^{RF} and H_{IG}^{RF} transfer functions show the same variability. The presence of double peaks in the IG range reflects possible harmonic behavior, which remains to be investigated (Sous et al., 2019). Present study observations show that the VLF waves have a mean period of 18 min, which differs slightly from the first seiche mode estimated at 15 min using the dimensions of the reef system. The expected variation of the mean period of VLF waves with the water depth is not observed, further encouraging a deeper mechanistic study of these wave components.

5.4. Setup

Setup increases for increasing offshore significant wave heights, but is also (to a lesser extent) modulated by the water level. Indeed, a slight decrease in setup occurs at high tide, whilst low tide leads to a slight increase in setup,

as previously observed (Becker et al., 2014; Bonneton et al., 2007; Sous, Dodet, et al., 2020). A rather straightforward explaination is that a lower water level leads to more breaking at the reef crest and an increased setup. Setup is largely forced by the breaking of GW over the reef, predicting 98% of the variance of the setup in the reef (cf. Table 3), that scales at 18% of the reef slope wave height, thus ranging from 0 to 0.8 m for 0–4 m of incident wave height. The tide only contributes for 2% of the setup variability (Figure 9c and Table 3). This corroborates the high correlation between setup and incident wave heights observed in a shore-attached fringing reef by Vetter et al. (2010). Other attempts have relied on the wave height and its product with wavelength to predict setup (e.g., Bonneton et al., 2007; Sous, Dodet, et al., 2020).

5.5. XBeach Model Validation

The XBeach numerical model allows to predict wave runup and the potential flood risk at the shoreline. Results show that with calibrated f_w and c_f values, the wave model is able to reproduce crossreef gravity and IG wave transformation processes. The $f_w = 0.3$ value adapted for XBeach simulations is close to the $f_w = 0.2$ value inferred by our observations and the Lentz et al. (2016) formulation. Such small differences between both values can find some explanation in the difficulty to numerically resolve bottom friction over a complex small-scale coral reef (Sous, Bouchette, et al., 2020; van Dongeren et al., 2013). The XBeach model performs best for the reproduction of gravity wave dissipation over the reef ($R^2 = 0.90$ against the field data, cf. Figure 7b). Good results are also observed for IG waves ($R^2 = 0.88$ against the field data, cf. Figure 7c). In the more extreme wave conditions, such as during P3 (cf. Figure 7h), the model underestimates H_{IG}^{RF} values by approximately 25% relative to the field data. Transformation of the annually dominant and shore normal Southern Ocean swell over the reef is well represented by the 1-D surfbeat mode XBeach configuration, as found in similar studies (e.g., Quataert et al., 2015; Lashley et al., 2018).

The XBeach model seems unable to correctly reproduce VLF amplification in the reef flat ($R^2 = 0.41$) observed from the field data. It could be that the transfer of energy to lower frequency bands or the reflection of the IG waves at the shore are not sufficiently reproduced to generate a resonant mechanism of the measured intensity. This could be explored using the short wave-resolving non-hydrostatic version of the XBeach model (e.g., Pearson et al. (2017); Scott et al. (2020)). In our study, the weaker model prediction of H_{VLF}^{RF} was initially attributed to the frequency at which new incident waves and tide are applied at the offshore boundary of the domain. Indeed, during the first simulations, these forcings were applied at the boundary every 10 min, resulting in the too frequent reinitialization of the free surface for the full development of VLF waves. However, modifications to allow for a delay of 60 min or 180 min between each forcing do not improve VLF height prediction, only their periods. During these tests, noise in the surface height variations also increased with the increase in forcing delay. As a result, the 10 min forcing intervals were kept for the present paper. In addition to the use of the short wave-resolving non-hydrostatic mode, the future use of a 2-D model configuration may also allow us to study the contributions of possible alongshore circulation and wave propagation in the reef to the reef hydrodynamics, though this requires experimental validation.

Though the incident conditions and the wave dissipation are well simulated, as well as setup during mild conditions, setup is underestimated in high energy wave events, by a maximum of 25% during the P3 extreme event (cf. Figure 7j). Buckley et al. (2015) give a first possible explanation for this using laboratory experiments. They find that the use of linear wave theory to calculate the radiation stress gradients leads to underpredicted setup, especially for cases with higher wave heights and lower still water levels, corresponding with our P3 event (cf. Table 1). A second possible explanation of the error in predicted setup for strong offshore wave conditions could be explained by the absence of 3D current shear in the presented simulations despite the resolution of wave setup (Guérin et al., 2018), during intense during extreme events especially. Guérin et al. (2018) numerically show that for a 1:20 slope, the contribution of such vertical processes in the surf zone could lead to a 20% increase of the total setup, and this effect is expected to increase with beach slope (1:10 in the present study).

5.6. Predicted Runup

The simulated runup is shown to be primarily driven by setup, and can be predicted by a transfer function using the offshore wave height and water level ($R^2 = 0.94$, Figure 9f). This function shows that 79% of the runup variability

is explained by the incident wave conditions, and 21% is explained by the tide. Runup, mainly composed of setup and swash, is modulated by the tide with which it is in antiphase at semidiurnal timescales (cf. Figure 8), as lower water levels at the reef flat lead to increased setup, and higher water levels at the reef flat lead to lower setup. As a rule of thumb, runup roughly scales as 20% of incident wave height. Since setup is the main contributor to the water level at the shoreline (cf. Table 2), and setup is shown to be underestimated for strong wave heights as the P3 event observed during the present study, the maximum computed runup of approximately 1 m (cf. Figure 8c) might also be underestimated. Thus, even if the offshore GW energy is highly dissipated and incident GW heights are clearly reduced on the reef flat, our results show that strong setup and runup (about 1 m for 4 m wave height) can be expected in the fringing reef of La Saline and the adjacent shoreline. Such setup and runup increase have already been evidenced and supposed to be enhanced for steep reef environments (Becker et al., 2014; Buckley et al., 2015; Gawehn et al., 2016; Pearson et al., 2017; A. C. N. Péquignet et al., 2009; Quataert et al., 2015). The occurrence of large wave height to water depth ratios at the breakpoint, similar to the conditions observed during the P3 event of this study, results in larger radiation stress gradients in shallow water and the transfer of kinetic energy into even shallower water. This may enhance setup on steep fore reef slopes (Buckley et al., 2015). IG waves at the shore can be reflected and then trapped on the reef flat if outgoing low-frequency waves are reflected again at the reef crest. This process depends on reef geometry and can result in resonant amplification of wave motions that may enhance runup (e.g., Gawehn et al., 2016; Pearson et al., 2017).

5.7. Implications for Stake-Holders

The present study produces reliable empirical formulations allowing to predict IG wave heights, setup, and runup at the reef flat, using offshore significant wave heights and water level fluctuations. These two offshore variables can be easily retrieved via open-access datasets. The offshore wave heights can be downloaded at a regional scale from the WaveWatch III numerical model or at a local scale from the French National Network CANDHIS (http://candhis.cetmef.developpement-durable.gouv) which operates a nearshore wave buoy and provides public access to real time and archived data (see Figure 1 for the localization of these two points of accessible data). In a similar way, the offshore tide can be retrieved through public access at Hydrographical Service of French Marine Shom website (www.data.shom.fr).

The runup (cf. Equation 12) and setup (cf. Equation 11) formulations derived in this study have the most relevant outcome for the civil society and stakeholders because it enables the fast, reliable prediction of nearshore water levels for coastal flood risk assessment. The proposed transfer functions are calibrated for significant wave heights reaching 4.5 m at the reef slope during SSW Southern Ocean swell, and water depths above the reef crest comprised between up to 1.5 m, covering a wide range of conditions. Several previous studies have developed tools for use in early warning systems or risk assessment, or to make projections about how wave-induced flooding on coral reef-lined coasts may change as a result of climate change (e.g., Rueda et al. (2019); Scott et al. (2020)). Such tools may provide a useful basis for comparison with the results from our study. For example, Pearson et al. (2017) developed Bayesian Estimator for Wave Attack in Reef Environments (BEWARE) ("Bayesian Estimator for Wave Attack in Reef Environments"), a large synthetic reef hydrodynamics database created with the same process-based hydrodynamics model used in the present study, XBeach, but in wave-resolving mode (XBeach Non-Hydrostatic,"XBNH"). To construct this database, Pearson et al. (2017) used idealized bathymetry and reef morphologies, commonly encountered in the field. In Figure 10, we compare BEWARE runup estimates for similar reef geometry to the one of La Saline fringing reef (i.e., an idealized bathymetry with a 500 m reef width, a 1:20 reef slope and a 1:10 beach slope, a coefficient of friction $c_f = 0.05$) to present study runup predictions using Equation 12. Comparison shows a good match between both. This raises the question of whether accounting for the full architectural complexity of a fringing coral reef is completely necessary for the satisfactory prediction of runup. Even if a number of studies (e.g., van Dongeren et al., 2013; Quataert et al., 2015; Lentz et al., 2016; Harris et al., 2018) suggest that local studies are necessary in order to consider the real reef structural complexity, specific to each reef, our results compared to the results issued from the database of Pearson et al. (2017) suggest that idealized configurations of reef systems with good friction parameterization should be enough to reproduce the water level in the reef flat (setup) or at the shore (runup). The present study lies in the low range of runup values of BEWARE (reaching approximately 1 m in Figure 10). This comparison could be extended to a wider range of values in the future, and runup estimates could be validated using field measurements.

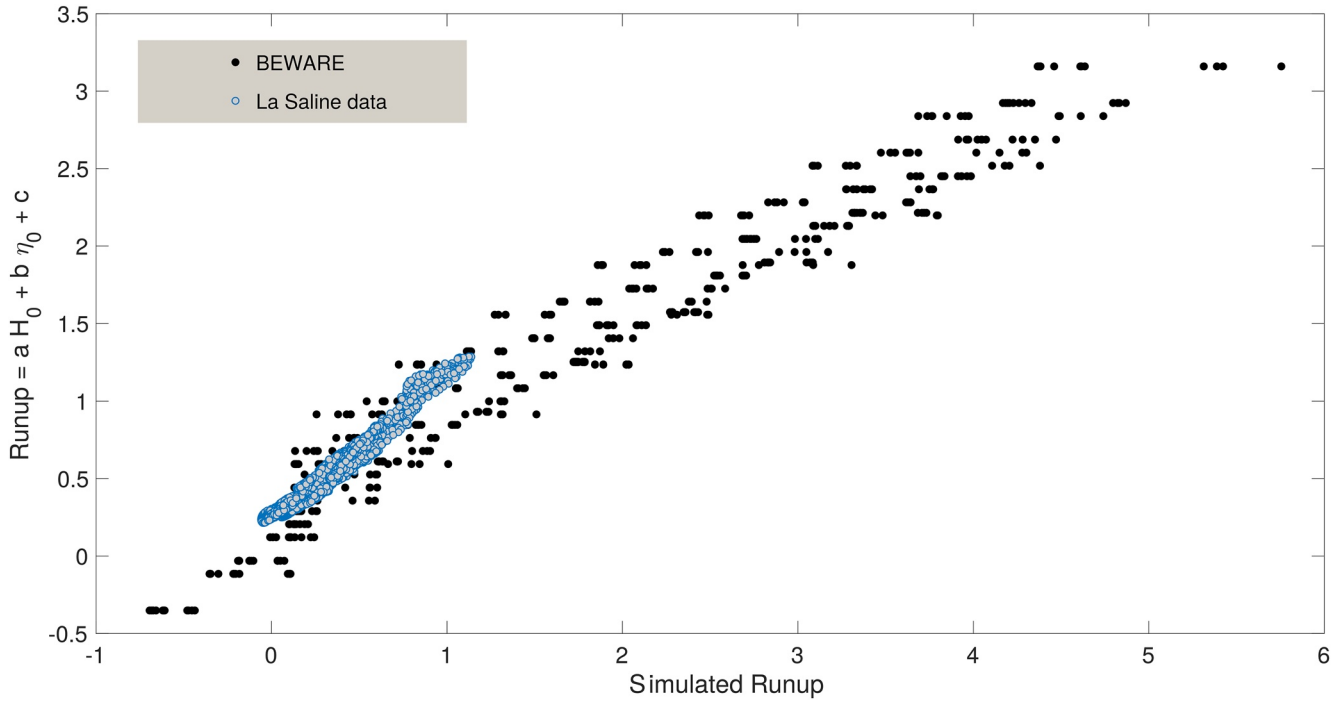

Figure 10. Comparison of the simulated runup from the presented configuration of this study and from Bayesian Estimator for Wave Attack in Reef Environments (BEWARE) (Pearson et al., 2017) to the transfer function calibrated in this study (Equation 12, Table 3). The BEWARE data points correspond to an idealized bathymetry with 500 m reef width, $c_f = 0.05$, a 1/20 reef slope and a 1/10 beach slope. H_0 and η_0 are, respectively, the offshore significant wave height and the offshore water level, as denoted by Pearson et al. (2017).

Even if La Saline is in a microtidal environment, the geometric configuration of reefs with a shallow reef crest leads to an enhanced influence of the water level. The water level modulates the breaking and the bed dissipation. For the moment, the water level oscillates close to the reef crest, since the coral has grown and kept pace with the sea level rise to date. However, under accelerated sea level rise scenarios, the coral may not be able to grow fast enough to keep up. As a consequence, the water depth above the crest will increase, breaking fewer waves and permitting more GW to cross the reef flat (cf. Figure 5), leading to potentially higher runup (cf. Figure 8, P3) and greater flooding.

The potential impact of climate change can also be considered by adopting a median sea level rise of 50 cm (projected for 2081–2100 according to the scenario RCP4.5 with moderate emission trajectories (IPCC report – Hoegh-Guldberg et al. (2014)). A 50 cm increase in mean water depth at the reef flat D would result in a mean increase of wave heights and runup in the reef system, such as a reef flat signficant wave height $H_{GW}^{RF} = 50$ cm for 4 m offshore significant wave height. Furthermore, the setup over the reef flat, which is expected to decrease as D decreases, could become less dominant in the La Saline reef hydrodynamics. Extrapolating from the proposed transfer functions (cf. Table 3) IG significant wave height would increase by 9 cm, and beach runup by 30 cm. In the case of an event similar to P3, this will lead to an added runup of 1.26 m, thus enhancing sediment erosion and the likelihood of flooding inland. Moreover, the possible decrease in the coral cover and complexity with climate change (Camp et al., 2018; Harris et al., 2018; Hoegh-Guldberg et al., 2014) could induce a decrease of the reef's friction factor, which is shown to decay the wave height more than twice the wave decay induced by the wave breaking only (considering only $\gamma = 0.55$ instead of analytical model, Equation 6). The resulting reduction of friction over the reef could accentuate the wave height increase, the runup increase, and the setup decrease in the reef system resulting from mean water level increase.

6. Conclusion

The present paper reports on a 2-month long field experiment at La Saline fringing reef, La Réunion, France. An array of pressure sensors was deployed along a single cross-shore transect to study wave transformation over the fringing reef, for Southern Ocean swell conditions that dominate the local annual wave climate. Offshore

significant wave heights range up to 4.36 m, and peak wave periods reach a maximum of 19 s. A series of numerical simulations performed with XBeach allow to further explain the hydrodynamic processes at play, and to simulate wave runup. The gravity wave and IG wave transformation is accurately reproduced by the XBeach 1-D surfbeat model configuration.

Reef hydrodynamics are found to depend on offshore gravity wave heights, and the tides to a lesser extent. The study reveals strong gravity wave attenuation across the fringing reef, acting as a low-pass filter, combined with high energy transfer to lower frequencies in the IG and VLF bands. The XBeach model underestimates VLF wave heights. As a result of the strong gravity wave energy dissipation, the reef hydrodynamics are dominated by setup, reaching 0.86 m (roughly 18% of incident significant wave height at the reef slope), and constituting the major contributor to wave runup (explaining approximately 67.9%). The present study proposes simple-to-use transfer functions to linearly combine contributors such as the water level and incident wave for the accurate prediction of reef flat hydrodynamics, such as setup and runup. With the rise in sea level and decline in coral health, the protective capacity of the La Saline reef could be reduced in the decades to come.

Data Availability Statement

The data used for the present study is available at https://geosur.osureunion.fr/geonetwork/srv/fre/catalog.search#/metadata/8bdc557b-e353-4d0a-bd45-1eb5f799752e. as well as https://sextant.ifremer.fr/record/aa42cbc1-c0cf-413e-b93d-8d0d1cbb0e06/.

Acknowledgments
This work was supported by the CALHYCO research program, the Geosciences Ocean lab (UMR6538) and the Geosciences Laboratory of La Reunion (UMR 7154). We are also thankful for the LabexMER (ANR-10-LABX-19) and ISblue project (Interdisciplinary graduate school for the blue planet - ANR-17-EURE-0015) research grants. Finally, this work was co-funded by the council of La Réunion Island and a "Investissements d'Avenir" French government grant.

References

Ardhuin, F., Rawat, A., & Aucan, J. (2014). A numerical model for free infragravity waves: Definition and validation at regional and global scales. *Ocean Modelling*, *77*, 20–32. https://doi.org/10.1016/j.ocemod.2014.02.006

Baldock, T. E., Karampour, H., Sleep, R., Vyltla, A., Albermani, F., Golshani, A., et al. (2014). Resilience of branching and massive corals to wave loading under sea level rise - a coupled computational fluid dynamics-structural analysis. *Marine Pollution Bulletin*, *86*(1–2), 91–101. https://doi.org/10.1016/j.marpolbul.2014.07.038

Baumann, J. H., Ries, J. B., Rippe, J. P., Courtney, T. A., Aichelman, H. E., Westfield, I., & Castillo, K. D. (2019). Nearshore coral growth declining on the mesoamerican barrier reef system. *Global Change Biology*, *25*(11), 3932–3945. https://doi.org/10.1111/gcb.14784

Becker, J. M., Merrifield, M. A., & Ford, M. (2014). Water level effects on breaking wave setup for Pacific island fringing reefs. *Journal of Geophysical Research: Oceans*, *119*(2), 914–932. https://doi.org/10.1002/2013jc009373

Beetham, E., & Kench, P. (2018). Predicting wave overtopping thresholds on coral reef-island shorelines with future sea-level rise. *Nature Communications*, *9*(1), 1–8. https://doi.org/10.1038/s41467-018-06550-1

Beetham, E., Kench, P. S., O'Callaghan, J., & Popinet, S. (2016). Wave transformation and shoreline water level on Funafuti atoll, t uvalu. *Journal of Geophysical Research: Oceans*, *121*(1), 311–326. https://doi.org/10.1002/2015jc011246

Bertin, X., De Bakker, A., Van Dongeren, A., Coco, G., André, G., Ardhuin, F., et al. (2018). Infragravity waves: From driving mechanisms to impacts. *Earth-Science Reviews*, *177*, 774–799. https://doi.org/10.1016/j.earscirev.2018.01.002

Bishop, C. T., & Donelan, M. A. (1987). Measuring waves with pressure transducers. *Coastal Engineering*, *11*(4), 309–328. https://doi.org/10.1016/0378-3839(87)90031-7

Bonneton, P., Lefebvre, J.-P., Bretel, P., Ouillon, S., & Douillet, P. (2007). Tidal modulation of wave-setup and wave-induced currents on the aboré coral reef, New Caledonia. *Journal of Coastal Research*, 762–766.

Brander, R. W., Kench, P. S., & Hart, D. (2004). Spatial and temporal variations in wave characteristics across a reef platform, Warraber Island, Torres Strait, Australia. *Marine Geology*, *207*(1–4), 169–184. https://doi.org/10.1016/j.margeo.2004.03.014

Buckley, M. L., Lowe, R. J., Hansen, J. E., & Van Dongeren, A. R. (2015). Dynamics of wave setup over a steeply sloping fringing reef. *Journal of Physical Oceanography*, *45*(12), 3005–3023. https://doi.org/10.1175/jpo-d-15-0067.1

Butt, T., & Russell, P. (2000). Hydrodynamics and cross-shore sediment transport in the swash-zone of natural beaches: A review. *Journal of Coastal Research*, 255–268.

Camp, E. F., Schoepf, V., Mumby, P. J., Hardtke, L. A., Rodolfo-Metalpa, R., Smith, D. J., & Suggett, D. J. (2018). The future of coral reefs subject to rapid climate change: Lessons from natural extreme environments. *Frontiers in Marine Science*, *5*, 4. https://doi.org/10.3389/fmars.2018.00433

Cheriton, O. M., Storlazzi, C. D., & Rosenberger, K. J. (2016). Observations of wave transformation over a fringing coral reef and the importance of low-frequency waves and offshore water levels to runup, overwash, and coastal flooding. *Journal of Geophysical Research: Oceans*, *121*(5), 3121–3140. https://doi.org/10.1002/2015jc011231

Chevalier, C., Sous, D., Devenon, J.-L., Pagano, M., Rougier, G., & Blanchot, J. (2015). Impact of cross-reef water fluxes on lagoon dynamics: A simple parameterization for coral lagoon circulation model, with application to the ouano lagoon, New Caledonia. *Ocean Dynamics*, *65*(11), 1509–1534. https://doi.org/10.1007/s10236-015-0879-x

Cordier, E., Lézé, J., & Join, J. L. (2013). Natural tidal processes modified by the existence of fringing reef on La Reunion Island (Western Indian Ocean): Impact on the relative sea level variations. *Continental Shelf Research*, *55*, 119–128. https://doi.org/10.1016/j.csr.2013.01.016

Cordier, E., Poizot, E., & Méar, Y. (2012). Swell impact on reef sedimentary processes: A case study of the La reunion fringing reef. *Sedimentology*, *59*(7), 2004–2023. https://doi.org/10.1111/j.1365-3091.2012.01332.x

Davy, C., Barruol, G., Fontaine, F., & Cordier, E. (2016). Analyses of extreme swell events on La Réunion Island from microseismic noise. *Geophysical Journal International*, *207*(3), 1767–1782. https://doi.org/10.1093/gji/ggw365

De Ridder, M. P., Smit, P. B., vanDongeren, A. R., McCall, R. T., Nederhoff, K., & Reniers, A. J. (2021). Efficient two-layer non-hydrostatic wave model with accurate dispersive behaviour. *Coastal Engineering*, *164*, 103808. https://doi.org/10.1016/j.coastaleng.2020.103808

Ferrario, F., Beck, M. W., Storlazzi, C. D., Micheli, F., Shepard, C. C., & Airoldi, L. (2014). The effectiveness of coral reefs for coastal hazard risk reduction and adaptation. *Nature Communications*, *5*(1), 1–9. https://doi.org/10.1038/ncomms4794

Gawehn, M., vanDongeren, A., vanRooijen, A., Storlazzi, C. D., Cheriton, O. M., & Reniers, A. (2016). Identification and classification of very low frequency waves on a coral reef flat. *Journal of Geophysical Research: Oceans*, *121*(10), 7560–7574. https://doi.org/10.1002/2016JC011834

Gerritsen, F. (1980). Wave attenuation and wave set-up on a coastal reef. In *Coastal engineering 1980* (pp. 444–461).

Grady, A., Moore, L., Storlazzi, C. D., Elias, E., & Reidenbach, M. (2013). The influence of sea level rise and changes in fringing reef morphology on gradients in alongshore sediment transport. *Geophysical Research Letters*, *40*(12), 3096–3101. https://doi.org/10.1002/grl.50577

Guedes, R. M., Bryan, K. R., & Coco, G. (2013). Observations of wave energy fluxes and swash motions on a low-sloping, dissipative beach. *Journal of Geophysical Research: Oceans*, *118*(7), 3651–3669. https://doi.org/10.1002/jgrc.20267

Guérin, T., Bertin, X., Coulombier, T., & deBakker, A. (2018). Impacts of wave-induced circulation in the surf zone on wave setup. *Ocean Modelling*, *123*, 86–97. https://doi.org/10.1016/j.ocemod.2018.01.006

Harris, D. L., Rovere, A., Casella, E., Power, H., Canavesio, R., Collin, A., et al. (2018). Coral reef structural complexity provides important coastal protection from waves under rising sea levels. *Science Advances*, *4*(2), eaao4350. https://doi.org/10.1126/sciadv.aao4350

Hoegh-Guldberg, O., Cai, R., Poloczanska, E. S., Brewer, P. G., Sundby, S., Hilmi, K., et al. (2014). The ocean. Climate change 2014: Impacts, adaptation, and vulnerability, Part B: Regional aspects. Chapter 30.

Hoegh-Guldberg, O., Mumby, P. J., Hooten, A. J., Steneck, R. S., Greenfield, P., Gomez, E., et al. (2007). Coral reefs under rapid climate change and ocean acidification. *Science*, *318*(5857), 1737–1742. https://doi.org/10.1126/science.1152509

Holthuijsen, L. H. (2010). *Waves in oceanic and coastal waters*. Cambridge university press.

Hom-ma, M., Horikawa, K., & Komori, S. (1966). Response characteristics of underwater wave gauge. *Coastal Engineering in Japan*, *9*(1), 45–54. https://doi.org/10.1080/05785634.1966.11924671

Hughes, T. P., Anderson, K. D., Connolly, S. R., Heron, S. F., Kerry, J. T., Lough, J. M., et al. (2018). Spatial and temporal patterns of mass bleaching of corals in the anthropocene. *Science*, *359*(6371), 80–83. https://doi.org/10.1126/science.aan8048

Hughes, T. P., Baird, A. H., Bellwood, D. R., Card, M., Connolly, S. R., Folke, C., et al. (2003). Climate change, human impacts, and the resilience of coral reefs. *Science*, *301*(5635), 929–933. https://doi.org/10.1126/science.1085046

Hughes, T. P., Kerry, J. T., Álvarez-Noriega, M., Álvarez-Romero, J. G., Anderson, K. D., Baird, A. H., et al. (2017). Global warming and recurrent mass bleaching of corals. *Nature*, *543*(7645), 373–377. https://doi.org/10.1038/nature21707

Lashley, C. H., Roelvink, D., vanDongeren, A., Buckley, M. L., & Lowe, R. J. (2018). Nonhydrostatic and surfbeat model predictions of extreme wave run-up in fringing reef environments. *Coastal Engineering*, *137*, 11–27. https://doi.org/10.1016/j.coastaleng.2018.03.007

Lentz, S., Churchill, J., Davis, K., Farrar, J., Pineda, J., & Starczak, V. (2016). The characteristics and dynamics of wave-driven flow across a platform coral reef in the red sea. *Journal of Geophysical Research: Oceans*, *121*(2), 1360–1376. https://doi.org/10.1002/2015jc011141

Lowe, R. J., & Falter, J. L. (2015). Oceanic forcing of coral reefs. *Annual Review of Marine Science*, *7*(1), 43–66. https://doi.org/10.1146/annurev-marine-010814-015834

Lowe, R. J., Falter, J. L., Bandet, M. D., Pawlak, G., Atkinson, M. J., Monismith, S. G., & Koseff, J. R. (2005). Spectral wave dissipation over a barrier reef. *Journal of Geophysical Research*, *110*(C4), C04001. https://doi.org/10.1029/2004JC002711

Lowe, R. J., Falter, J. L., Koseff, J. R., Monismith, S. G., & Atkinson, M. J. (2007). Spectral wave flow attenuation within submerged canopies: Implications for wave energy dissipation. *Journal of Geophysical Research*, *112*(C5), C05018. https://doi.org/10.1029/2006jc003605

Mahabot, M.-M., Pennober, G., Suanez, S., Troadec, R., & Delacourt, C. (2017). Effect of tropical cyclones on short-term evolution of carbonate sandy beaches on reunion island, indian ocean. *Journal of Coastal Research*, *33*(4), 839–853. https://doi.org/10.2112/jcoastres-d-16-00031.1

McLean, R., & Kench, P. (2015). Destruction or persistence of coral atoll islands in the face of 20th and 21st century sea-level rise? *Wiley Interdisciplinary Reviews: Climate Change*, *6*(5), 445–463. https://doi.org/10.1002/wcc.350

Merrifield, M., Becker, J., Ford, M., & Yao, Y. (2014). Observations and estimates of wave-driven water level extremes at the Marshall Islands. *Geophysical Research Letters*, *41*(20), 7245–7253. https://doi.org/10.1002/2014gl061005

Michel, R., Pascal, M., Touria, B., & Christophe, D. (2016). HYSCORES: Cartographies hyperspectrales appliquées aux écosystèmes coralliens et à leurétat de santé. (Tech. Rep.). *Ifremer Délegation Ocean Indien*. https://doi.org/10.13155/46122

Monismith, S. G., Herdman, L. M., Ahmerkamp, S., & Hench, J. L. (2013). Wave transformation and wave-driven flow across a steep coral reef. *Journal of Physical Oceanography*, *43*(7), 1356–1379. https://doi.org/10.1175/jpo-d-12-0164.1

Monismith, S. G., Rogers, J. S., Koweek, D., & Dunbar, R. B. (2015). Frictional wave dissipation on a remarkably rough reef. *Geophysical Research Letters*, *42*(10), 4063–4071. https://doi.org/10.1002/2015GL063804

Mouquet, P., Bajjouk, T., & Ropert, M. (2016). MNT Bathymétrique à haute résolution des fonds marins des zones récifales de la côte ouest de l'île de La Réunion (2015). (Tech. Rep.). *Ifremer délégation Océan Indien*. https://doi.org/10.12770/ee059de2-2c81-46ce-88de-0fb5517046af

Owen, S., Kench, P., & Ford, M. (2016). Improving understanding of the spatial dimensions of biophysical change in atoll island countries and implications for island communities: A Marshall Islands' case study. *Applied Geography*, *72*, 55–64. https://doi.org/10.1016/j.apgeog.2016.05.004

Pascal, N., Allenbach, M., Brathwaite, A., Burke, L., Le Port, G., & Clua, E. (2016). Economic valuation of coral reef ecosystem service of coastal protection: A pragmatic approach. *Ecosystem Services*, *21*, 72–80. https://doi.org/10.1016/j.ecoser.2016.07.005

Pearson, S., Storlazzi, C. D., Van Dongeren, A., Tissier, M., & Reniers, A. (2017). A bayesian-based system to assess wave-driven flooding hazards on coral reef-lined coasts. *Journal of Geophysical Research: Oceans*, *122*(12), 10099–10117. https://doi.org/10.1002/2017jc013204

Pedersen, T. (2002). Wave measurements using the PUV method (Technical Report No. 1). *Nortek Group*.

Péquignet, A.-C., Becker, J. M., Merrifield, M., & Boc, S. (2011). The dissipation of wind wave energy across a fringing reef at ipan, Guam. *Coral Reefs*, *30*(1), 71–82. https://doi.org/10.1007/s00338-011-0719-5

Péquignet, A.-C. N., Becker, J. M., & Merrifield, M. A. (2014). Energy transfer between wind waves and low-frequency oscillations on a fringing reef, Ipan, Guam. *Journal of Geophysical Research: Oceans*, *119*(10), 6709–6724. https://doi.org/10.1002/2014JC010179

Péquignet, A. C. N., Becker, J. M., Merrifield, M. A., & Aucan, J. (2009). Forcing of resonant modes on a fringing reef during tropical storm man-yi. *Geophysical Research Letters*, *36*(3), L03607. https://doi.org/10.1029/2008gl036259

Pierson, W. J., & Marks, W. (1952). The power spectrum analysis of ocean-wave records. *Eos, Transactions American Geophysical Union*, *33*(6), 834–844. https://doi.org/10.1029/tr033i006p00834

Pomeroy, A., Lowe, R., Symonds, G., vanDongeren, A., & Moore, C. (2012). The dynamics of infragravity wave transformation over a fringing reef. *Journal of Geophysical Research*, *117*(11), C11022. https://doi.org/10.1029/2012jc008310

Pomeroy, A., Lowe, R. J., Van Dongeren, A. R., Ghisalberti, M., Bodde, W., & Roelvink, D. (2015). Spectral wave-driven sediment transport across a fringing reef. *Coastal Engineering*, *98*, 78–94. https://doi.org/10.1016/j.coastaleng.2015.01.005

Principe, P., Bradley, P., Yee, S., Fisher, W., Johnson, E., Allen, P., & Campbell, D. (2011). *Quantifying coral reef ecosystem services*. U.S. Environmental Protection Agency.

Quataert, E., Storlazzi, C., Rooijen, A., Cheriton, O., & vanDongeren, A. (2015). The influence of coral reefs and climate change on wave-driven flooding of tropical coastlines. *Geophysical Research Letters*, *42*(15), 6407–6415. https://doi.org/10.1002/2015GL064861.Received

Quataert, E., Storlazzi, C., vanDongeren, A., & McCall, R. (2020). The importance of explicitly modelling sea-swell waves for runup on reef-lined coasts. *Coastal Engineering*, *160*, 103704. https://doi.org/10.1016/j.coastaleng.2020.103704

Roelvink, D., & Brøker, I. (1993). Cross-shore profile models. *Coastal Engineering*, *21*(1–3), 163–191. https://doi.org/10.1016/0378-3839(93)90049-e

Roelvink, D., McCall, R., Mehvar, S., Nederhoff, K., & Dastgheib, A. (2018). Improving predictions of swash dynamics in XBeach: The role of groupiness and incident-band runup. *Coastal Engineering*, *134*, 103–123. https://doi.org/10.1016/j.coastaleng.2017.07.004

Roelvink, D., Reniers, A., Van Dongeren, A., De Vries, J. V. T., McCall, R., & Lescinski, J. (2009). Modelling storm impacts on beaches, dunes and barrier islands. *Coastal Engineering*, *56*(11–12), 1133–1152. https://doi.org/10.1016/J.COASTALENG.2009.08.006

Rogers, J. S., Monismith, S. G., Koweek, D. A., & Dunbar, R. B. (2016). Wave dynamics of a Pacific a toll with high frictional effects. *Journal of Geophysical Research: Oceans*, *121*(1), 350–367. https://doi.org/10.1002/2015jc011170

Rueda, A., Cagigal, L., Pearson, S., Antolínez, J. A., Storlazzi, C., vanDongeren, A., et al. (2019). Hycreww: A hybrid coral reef wave and water level metamodel. *Computers & Geosciences*, *127*, 85–90. https://doi.org/10.1016/j.cageo.2019.03.004

Ruggiero, P., Komar, P. D., McDougal, W. G., Marra, J. J., & Beach, R. A. (2001). Wave runup, extreme water levels and the erosion of properties backing beaches. *Journal of Coastal Research*, 407–419.

Scott, F., Antolinez, J. A., McCall, R., Storlazzi, C., Reniers, A., & Pearson, S. (2020). Hydro-morphological characterization of coral reefs for wave runup prediction. *Frontiers in Marine Science*, *7*, 361. https://doi.org/10.3389/fmars.2020.00361

Sheppard, C., Dixon, D. J., Gourlay, M., Sheppard, A., & Payet, R. (2005). Coral mortality increases wave energy reaching shores protected by reef flats: Examples from the Seychelles. *Estuarine, Coastal and Shelf Science*, *64*(2–3), 223–234. https://doi.org/10.1016/j.ecss.2005.02.016

Shope, J. B., Storlazzi, C. D., & Hoeke, R. K. (2017). Projected atoll shoreline and run-up changes in response to sea-level rise and varying large wave conditions at wake and midway atolls, northwestern Hawaiian islands. *Geomorphology*, *295*, 537–550. https://doi.org/10.1016/j.geomorph.2017.08.002

Sous, D., Bouchette, F., Doerflinger, E., Meulé, S., Certain, R., Toulemonde, G., et al. (2020). On the small-scale fractal geometrical structure of a living coral reef barrier. *Earth Surface Processes and Landforms*, *45*(12), 3042–3054. https://doi.org/10.1002/esp.4950

Sous, D., Dodet, G., Bouchette, F., & Tissier, M. (2020). Momentum balance over a barrier reef. *Journal of Geophysical Research: Oceans*, *125*(2). https://doi.org/10.1029/2019jc015503

Sous, D., Tissier, M., Rey, V., Touboul, J., Bouchette, F., Devenon, J.-L., et al. (2019). Wave transformation over a barrier reef. *Continental Shelf Research*, *184*, 66–80. https://doi.org/10.1016/j.csr.2019.07.010

Storlazzi, C. D., Elias, E. P., & Berkowitz, P. (2015). Many atolls may be uninhabitable within decades due to climate change. *Scientific Reports*, *5*(1), 1–9. https://doi.org/10.1038/srep14546

Storlazzi, C. D., Gingerich, S. B., vanDongeren, A., Cheriton, O. M., Swarzenski, P. W., Quataert, E., et al. (2018). Most atolls will be uninhabitable by the mid-21st century because of sea-level rise exacerbating wave-driven flooding. *Science Advances*, *4*(4), eaap9741. https://doi.org/10.1126/sciadv.aap9741

Symonds, G., Black, K. P., & Young, I. R. (1995). Wave-driven flow over shallow reefs. *Journal of Geophysical Research*, *100*(C2), 2639–2648. https://doi.org/10.1029/94jc02736

Symonds, G., Huntley, D. A., & Bowen, A. J. (1982). Two-dimensional surf beat: Long wave generation by a time-varying breakpoint. *Journal of Geophysical Research*, *87*(C1), 492–498. https://doi.org/10.1029/jc087ic01p00492

UNESCO. (2014). Islands of the future — building resilience in a changing world. Retrieved from https://unesdoc.unesco.org/ark:/48223/pf0000224512

van Dongeren, A., Lowe, R., Pomeroy, A., Trang, D. M., Roelvink, D., Symonds, G., & Ranasinghe, R. (2013). Numerical modeling of low-frequency wave dynamics over a fringing coral reef. *Coastal Engineering*, *73*, 178–190. https://doi.org/10.1016/j.coastaleng.2012.11.004

van Dongeren, A., Roelvink, D., McCall, R., Nederhoff, K., & vanRooijen, A. (2017). Modeling the morphological impacts of coastal storms. *Coastal storms: Processes & Impacts*, 195–216.

Vetter, O., Becker, J. M., Merrifield, M. A., Pequignet, A.-C., Aucan, J., Boc, S. J., & Pollock, C. E. (2010). Wave setup over a Pacific island fringing reef. *Journal of Geophysical Research*, *115*(C12), C12066. https://doi.org/10.1029/2010jc006455

Woodhead, A. J., Hicks, C. C., Norström, A. V., Williams, G. J., & Graham, N. A. (2019). Coral reef ecosystem services in the Anthropocene. *Functional Ecology*, *33*(6), 1023–1034. https://doi.org/10.1111/1365-2435.13331